Review

Dicyanamide-perovskites at the edge of dense hybrid organic–inorganic materials

Javier García-Ben [a,b], Lauren Nicole McHugh [c], Thomas Douglas Bennett [c], Juan Manuel Bermúdez-García [a,b,c,*]

[a] Universidade da Coruña, Quimolmat, Centro de Investigacións Científicas Avanzadas (CICA), Rúa as Carballeiras, 15071, A Coruña, Spain
[b] Universidade da Coruña, Quimolmat, Departamento de Química, Facultade de Ciencias, Campus da Zapateira, 15008, A Coruña, Spain
[c] University of Cambridge, Department of Materials Science and Metallurgy, Cambridge CB3 0FS, United Kingdom

ARTICLE INFO

ABSTRACT

Hybrid organic–inorganic ABX_3 perovskites with dicyanamide-ligands (dca: $[N(CN)_2]^-$) on the X-site are emerging as a distinct group of materials courtesy of their multifunctional properties. Here we present an in-depth analysis of the members of this dicyanamide perovskite family, where the presence of the 5 atom-long dca ligand gives rise to relatively open crystal structures - especially when compared with other dense hybrids such as perovskite formates, and which has a profound influence on their chemistry and properties. We compile the synthetic procedures used to obtain these compounds, along with their chemical and structural properties. In terms of their functional properties, dicyanamide-perovskites have already shown an enormous potential for future applications, such as dielectric or magnetic switches, eco-friendly barocaloric refrigerants at low-pressure and room-temperature, or precursors for oil-recovery nanomaterials and thermoelectric glasses, as reviewed here. Additionally, we highlight several emerging phenomena in this family, and anticipate areas with room for development in the field.

Contents

HOIPs, hybrid organic-inorganic perovskites; MOFs, metal-organic frameworks; IUPAC, International Union of Pure and Applied Chemistry; DMF, N,N-dimethylformamide; dca, dicyanamide; Me, methyl; Et, ethyl; Pr, propyl; Bu, butyl; Bn, benzyl; Ph, phenyl; Cp*, pentamethylcyclopentadiene; AP, alkylphosphonium; M@CNTs, carbon nanotubes with embedded magnetic nanoparticles; AFM, antiferromagnetism; FM, ferromagnetism; NLO, nonlinear optical; LED, light emitting diode.

* Corresponding author.
  E-mail address: j.bermudez@udc.es (J.M. Bermúdez-García).

1. Introduction

The term perovskite was coined in 1839 by the Prussian mineralogist Gustav Rose, to define a new mineral of greyish to iron-black colour, which was composed of titanium and calcareous earth. The mineral was discovered in the Ural Mountains and has a hardness of 5.8 on the Mohs scale. Rose received the sample from one of his colleagues, the Russian mineralogist August Alexander Krämmerer, who requested that the mineral be named in honour of his fellow countryman and established mineralogist, the Count Lev Alexander Perovski [1]. This enigmatic mineral has the chemical composition $CaTiO_3$ and its crystal structure was first described by Victor Goldschmidt in his famous work on tolerance factors [2]. The structure was later reported from X-ray diffraction data collected on the isostructural $BaTiO_3$ compound by Helen Dick Megaw [3].

Nowadays, the term perovskite is used to refer to a vast number of isostructural inorganic compounds with general formula ABX_3, where A and B are cations of different size (A is larger than B), and X is an anion that is six-coordinated to the B cation, forming $[BX_6]$ octahedra, and twelve-coordinated to the A cation, forming $[AX_{12}]$ cuboctahedra (Fig. 1). In this formulism, A are normally alkali, alkaline earth metal cations or lanthanide cations, B are generally transition metal cations, and X may be anions such as sulphur, nitrogen, halide or oxygen anions [4]. Traditionally, perovskites have been classified by the X anion present in the structure. In that regard, the family of oxide perovskites has been probably the one most widely studied in the 20th century, even if halide-perovskites are now at the centre of a vast number of investigations [5–8].

As the properties of perovskites have been studied since the middle of the 20th century [9], the perovskite structure has been behind some of the most important scientific and technological achievements of our society. Among them, the discovery of high-temperature superconductivity in an oxide with a perovskite superstructure, for which J. Georg Bednorz and K. Alexander Müller were awarded the Nobel Prize in Physics in 1987 [10,11], which could be considered the first major scientific breakthrough involving perovskites [10,11]. Another example is the discovery of colossal magnetoresistance in manganese perovskites [12,13] or, even more recently, magnetoelectricity in several multiferroic perovskites [14].

Today, due to a wide range of multifunctional properties, and particularly their photovoltaic and optoelectronic properties [15,16], there is a renewed surge of activity into the so-called hybrid organic–inorganic perovskites (HOIPs). This term is used to embody those compounds that integrate organic and inorganic building-blocks in an extended perovskite-like structure. In this modified ABX_3 structure, the A cation is substituted by organic cations (normally alkylamine cations), B remains occupied by metal cations and X can be occupied either by halide anions or polyatomic bidentate-bridge ligands [7]. There are also some recent examples of metal-free HOIPs, where B is replaced by ammonium cations (NH_4^+) [17–20].

The synthesis of the first HOIPs may be attributed to H. Remy and G. Laves, who in 1933 reported a large family of alkylammonium copper chlorides, including the perovskite-like $[(CH_3)_4N][CuCl_3]$ compound [21]. However, the most widely studied HOIPs are those of general formula $[CH_3NH_3][PbX_3]$ ($X = Cl^-$, Br^- or I^-), reported for the first time by D. Weber in 1978 [22], and that in the last years have posed a breakthrough in the field of solar cells [15,16]. In the case of using a polyatomic bidentate-bridge ligand in the X-site, a large variety of HOIPs can be obtained, some of them with relevant functional properties.

For instance, when X is the formate ($HCOO^-$) ligand, the up to-date largest subclass of HOIPs is obtained [7,23–54]. These formate hybrids with perovskite architecture boosted research in the field, especially since antiferroelectric and multiferroic properties were described for members of this family [48,51,52]. Other populated families of HOIPs are those in which X are cyanide (CN^-) [55–64], azide (N_3^-) [65–72], and dicyanamide (dca or $N(CN)_2^-$) [73–85] bidentate-bridge ligands.

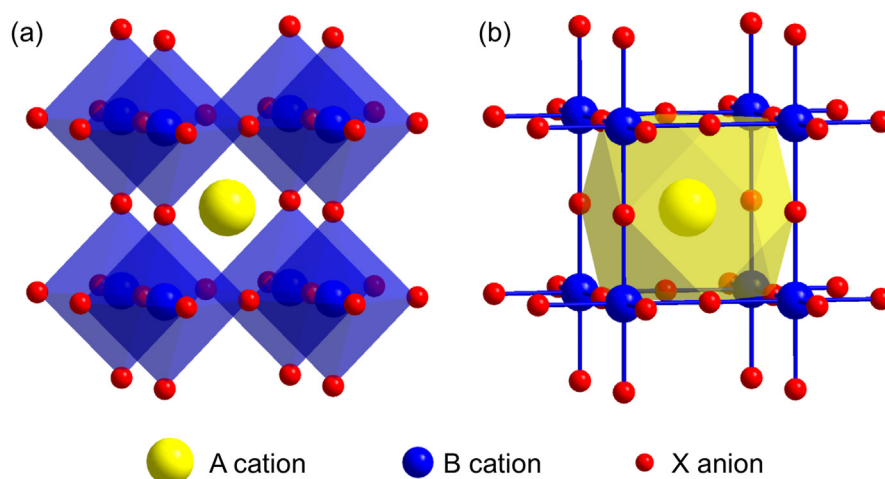**Fig. 1.** Crystal structure of a general ABX_3 perovskite, showing (a) $[BX_6]$ octahedral coordination and (b) $[AX_{12}]$ cuboctahedral coordination.

There are also a few examples of rare HOIPs where X is occupied by thiocyanate (SCN^-) [86,87], perchlorate (ClO_4^-) [88–91], hypophosphite (H_2POO^-) [92,93], tetrafluoroborate (BF_4^-) [19,88], borohydride (BH_4^-) [94], or dicyanometallate ($M(CN)_2^-$) [95,96] anions.

At this point, it should be distinguished that there are different types of chemical bonds in the 3D-framework between the B and X building-blocks. Some of these HOIPs exhibit bonds between B-metals and X-inorganic ligands (such as F^-, Cl^-, Br^-, I^-, CN^-, N_3^-, $N(CN)_2^-$, SCN^-, ClO_4^-, H_2POO^-, BF_4^-, BH_4^- and $M(CN)_2^-$). Meanwhile, others display bonds between B-metals and X-organic ligands (such as $HCOO^-$). According to C.N.R. Rao *et al.*, these two types of frameworks could be divided into I^3O^0 and I^0O^3 3D-coordination compounds, respectively [97]. In that regard, it should be also noted that halide perovskites are often referred as organometallic compounds, although this is a common inaccuracy. According to the IUPAC, organometallic compounds must display bonds between a metal and a carbon atom from an organic ligand, and that is not the case in the known HOIPs. [98–100].

In addition, HOIP structures (especially formate-HOIPs) are also often classified as metal–organic frameworks (MOFs) [33,39,46,52], given the existence of extended hybrid organic–inorganic bonding in both families. Nevertheless, the IUPAC definition of the latter [101,102] is "a coordination polymer (or alternatively coordination network) with an open framework containing potential voids". Most MOFs are, thus, considered porous materials [103–107], a feature which leads to a wide variety of technological applications, such as gas capture, storage and/or separation (i.e. CO_2, H_2 or natural gas) [108–110], water harvesting in dry environments [111,112], evaporative refrigeration [113,114], or drug delivery [115,116], to list only a few. Whilst the overwhelming majority of MOF structures are crystalline solids [103–106], there is an increasing emergence of non-crystalline MOFs, particularly in liquid and glass states [117,118]. It is also worth noting that most of MOF structures, due to their large void volume, are metastable once pore-occupying solvent molecules have been removed.

In contrast, HOIPs would be better categorized into the "coordination polymers" class, as they have minimal or negligible voids, which are inaccessible to exterior molecules. This characteristic makes HOIPs generally more stable than MOFs. Moreover, this lack of void space leads to an increased structural density, which allows for stronger atomic interactions and confers multifunctional properties, such as photovoltaic and optoelectronic properties [15,16], long-range ferroic order [51,53,61,77,119], and even type-I and type-II multiferroicity [29,33,39,52,80,120,121].

Up to now, there have been many excellent reviews on HOIPs [7,98,122–124]. However, none are specifically focused on the dicyanamide-perovskites subclass. For that reason, some important structural features that affect to the structural and functional properties have remained unnoticed. For example, as it will be discussed in the following paragraphs, when increasing the length of the X-ligand (from halides to dicyanamides), the voids of the pseudo-cubooctahedral cavities also increase and, therefore, they can allocate bigger A-cations with larger degrees of freedom. In turn, this will affect the structural disordering as well as the mechanical properties (increase of the elasticity modulus, the softness and the pressure-responsiveness), which will ultimately induce novel mechanisms (not observed in other HOIPs) for the appearance of functional properties (such as dielectric, magnetic and ferroelastic properties, multiferroicity, and/or low-pressure giant barocaloric effects). Additionally, the presence of the 5-atom long dca ligand in the X-site may give rise to somewhat open structures, which can be compared (up-to a certain level) to that of the MOFs. Furthermore, the presence of C- and N-rich X-ligands (and A-cations) make these compounds interesting precursors for carbon nanomaterials and glasses, property that is not observed in other HOIPs.

The purpose of our review is to provide a deep comparative study of the dicyanamide HOIP subfamily reported so far, and contrast them to the principal HOIPs and MOFs. As we will discuss, these compounds bear similarities not only with other denser HOIPs but also, and very interestingly, with porous MOFs, characteristics that render them a unique family at the edge of dense perovskites.

2. Synthesis methods

In general, the synthetic methods used to obtain dicyanamide-perovskites reported in literature are simple and relatively fast, with low-energy consumption, low toxicity and are a low risk to the operator. This is an important advantage in comparison with the methods used to prepare oxide- and halide-perovskites, which typically require high temperatures, more complex techniques, and/or hazardous solvents.

In the case of dicyanamide-perovskites, the synthetic routes can be broadly classified into three categories (Table 1): *layer-diffusion*, *slow evaporation* and *fast evaporation* methods.

The *layer-diffusion* method consists of adding two solutions with different densities in a sealed glass tube (vertical, U-shaped and/or H-shaped), which generates an interface between the two solutions. One of the solutions contains some of the starting reagents required for the synthesis, and the other solution contains the remaining components. All the chemicals then diffuse in the aforementioned interface, where they react to form the desired HOIP. This method generally slows the chemical reactions and allows for improved crystallization and the formation of larger single crystals [78–81,84,125–131].

The *slow evaporation* route uses a homogeneous mixture of two starting solutions containing the required reagents. This method is normally used when the two starting solutions have a similar density and they cannot form an interface. This route is generally a little faster than *layer-diffusion*, though it does lead to smaller single crystals [73–78,82,83,85].

The fast evaporation alternative is based on rapid elimination of the solvent, to force fast precipitation of the HOIP. In this route, the starting solutions are mixed together as in the slow evaporation method. The evaporation is however accelerated using a rotary evaporator, where the vacuum pressure and the temperature can be controlled [132]. This method consumes a slightly larger amount of energy due to the use of a rotary evaporator, though the HOIP is obtained more quickly in the form of a homogenous polycrystalline powder (which is often desired for specific applications) [132].

As previously mentioned, the first two procedures have longer reaction times, which can vary from a couple of days [78,126] to weeks [73,79,82], or even months [74]. In contrast, J.M. Bermúdez-García *et al.* obtained pure polycrystalline powders of $[Pr_4N][M(dca)_3]$ (M = Co^{2+}, Ni^{2+}) in minutes, using the *fast evaporation* method [132].

In general, the synthetic routes described above used aqueous solutions [76,85] or mixtures of H_2O with CH_3CH_2OH [128,129] or CH_3OH [75,83]. For the synthesis of the $[Cp^*_2M][M'(dca)_3]$ (M = Fe^{3+}, Co^{3+}; M' = Mn^{2+}, Fe^{2+}, Co^{2+}, Ni^{2+}, Cd^{2+}) however, P. M. Van der Werff *et al.* used different combinations of organic solvents (CH_3CH_2OH, CH_3CN or DMF) depending of the desired HOIP [78].

Even if only few references specify the yield obtained from their syntheses, the *fast evaporation* route for $[Pr_4N][M(dca)_3]$ (M = Co^{2+}, Ni^{2+}) provides the highest yield (around 95%) [132]. In the case of $[Bu_3BnN][M(dca)_3]$ (M = Mn^{2+}, Co^{2+}) and $[Et_3BnN][M(dca)_3]$ (M = Mn^{2+}, Fe^{2+}), which were obtained by *slow evaporation,* yields

Table 1
Synthesis methods reported for dicyanamide-perovskites.

Perovskite	Method	Solvent	A-cation origin	Time	Yield	Ref
[Cp*₂Co][M(dca)₃] (Cp* = C₅(CH₃)₅–; M = Co2+, Ni²⁺)	Layer-diffusion	CH₃CH₂OH + CH₃CN (9:1)	Selectively synthesized	Several days	–	[78]
[Cp*₂Fe][M(dca)₃] (Cp* = C₅(CH₃)₅–; M = Mn²⁺, Ni²⁺)	Layer-diffusion	CH₃CH₂OH	Selectively synthesized	5 days	–	[78]
[Pr₄N][M(dca)₃] (Pr = CH₃CH₂CH₂–; M = Mn²⁺, Fe²⁺, Co²⁺, Ni²⁺, Cd²⁺)	Layer-diffusion	CH₃CH₂OH + H₂O (10:20)	Commercially available	Few days to 2 weeks	–	[79–81, 84,124–129]
[Cp*₂Fe][M(dca)₃] (Cp* = C₅(CH₃)₅–; M = Mn²⁺, Fe²⁺, Co²⁺, Ni²⁺, Cd²⁺)	Slow evaporation	CH₃CH₂OH	Selectively synthesized	Several days	38 – 68%	[78]
[Cp*₂Fe][M(dca)₃] (Cp* = C₅(CH₃)₅–; M = Mn²⁺, Co²⁺, Ni²⁺, Cd²⁺)	Slow evaporation	CH₃CH₂OH	Selectively synthesized	Several days	39–63%	[78]
[Cp*₂Fe][Fe(dca)₃] (Cp* = C₅(CH₃)₅–)	Slow evaporation	CH₃CH₂OH + H₂O (3:1)	Selectively synthesized	Several days	68%	[78]
[Cp*₂Co][Mn(dca)₃] (Cp* = C₅(CH₃)₅–)	Slow evaporation	CH₃CH₂OH + DMF (25:5)	Selectively synthesized	24 h	32%	[78]
[Cp*₂Co][M(dca)₃] (Cp* = C₅(CH₃)₅–; M = Co²⁺, Ni²⁺)	Slow evaporation	CH₃CH₂OH + CH₃CN (25:5)	Selectively synthesized	24 h	50 – 57%	[78]
[R₃BnN][M(dca)₃] (Bn = C₅H₄C–; R = CH₃CH₂–, CH₃CH₂CH₂–; M = Mn²⁺, Fe²⁺, Co²⁺)	Slow evaporation	CH₃OH + H₂O (10:5)	Commercially available	2 weeks	70–90%	[73]
[Et₃RP][Mn(dca)₃] (R = CH₃CH₂CH₂–, CH₂CHCH₂–, CH₃OCH₂–)	Slow evaporation	CH₃OH+ H₂O	Selectively synthesized	Several days	–	[83]
[Et₃(n-Pr)P][Cd(dca)₃] (Pr = CH₃CH₂CH₂–)	Slow evaporation	CH₃OH+ H₂O	Selectively synthesized	2 weeks	–	[82]
[Et₃(CH₂CH₂X)P][M(dca)₃] (X = F⁻, Cl⁻; M = Mn²⁺, Cd²⁺)	Slow evaporation	H₂O	Selectively synthesized	–	–	[76,85]
[Ph₃S][Mn(dca)₃] (Ph = C₆H₅–)	Slow evaporation	CH₃CH₂OH + H₂O (10:20)	Commercially available	2 months	–	[74]
[Bu₃MeN][M(dca)₃] (Bu = CH₃CH₂CH₂CH₂–; M = Mn²⁺, Fe²⁺, Co²⁺, Ni²⁺)	Slow evaporation	CH₃OH + H₂O (20:10)	Commercially available	1 week	–	[75]
[Pr₃RN][Mn(dca)₃] (Pr = CH₃CH₂CH₂–; R = CH₃CHCH₂OH–, CH₂CHOHCH₃–)	Slow evaporation	H₂O	Selectively synthesized	–	–	[77]
[Pr₄N][M(dca)₃] (Pr = CH₃CH₂CH₂–; M = Co²⁺, Ni²⁺)	Fast evaporation (rotavap)	CH₃CH₂OH + H₂O	Commercially available	Few minutes	∼95%	[132]

of between 70 and 90% have been achieved [73]. Meanwhile, the [Cp*₂M][M'(dca)₃] (M = Fe³⁺, Co³⁺; M' = Mn²⁺, Fe²⁺, Co²⁺, Ni²⁺, Cd²⁺) compounds present lower yields of between 32 and 68% [78].

Another important point in the synthetic routes is the origin and availability of the building-blocks that configure the designed HOIPs. In this context, the metals that occupy the B-site cations and the dca X-ligands are widely available from commercial reagents. However, for the A-site cations, some are commercially available, though many others are specifically designed in size and shape to fit into the perovskite cubooctahedral cavities (see Table 1).

3. Structural analysis of the dicyanamide-perovskite family

3.1. General structure

The dca anion, [N≡C-N-C≡N]⁻, is a very versatile ligand with one central N–amide atom and two end -C≡N cyanide groups. Since it was first used by Köhler *et al.* to obtain non-molecular solids [133], it has been widely employed to obtain novel chemical architectures and compounds, some of which display long-range magnetic coupling between metals [134].

This conjugated long anion displays three different N–coordination centres that can provide up to eight coordination modes with different denticity, as shown in Fig. 2 [134]. In the literature, a short nomenclature for each one of the coordination modes is often found. This nomenclature uses the symbol "μ" (which indicates coordination) followed by numbers that indicate the position where the dca ligand is linked with a given metal (where 1 and 5 indicate coordination through the N-cyanide atoms, and 3 indicates coordination through the N-amide atom). In that way, the dca ligands can be monodentate coordinating through one of the N–cyanide ends (μ₁) or through the N-amide atom (μ₃). Moreover,

this anion can also act as a bidentate–bridge ligand when coordinating through the two N-cyanide ends (μ₁,₅) or through one of the N-cyanide atoms and the N-amide (μ₁,₃). And even more, in some cases, the dca ligand can present tridentate (μ₁,₃,₅ or μ₁,₁,₅), tetradentate (μ₁,₁,₃,₅) or pentadentate (μ₁,₁,₃,₅,₅) coordination modes.

Alternatively, and according to the IUPAC, the extended nomenclature for these coordination modes will use the symbol "μₙ" to represent the denticity of the ligand (where "n" shows the number of metals linked to the ligand) and the symbol "ηⁿ" to indicate the hapticity of each N-atom (where "n" shows the number of metals linked to the given N-atom) [135,136]. Herein, as a matter of example, a pentadentate dca ligand can be defined as "μ₁,₁,₃,₅,₅" in the traditional short nomenclature or "μ₅ - η²:η¹:η²" in the normative IUPAC nomenclature.

In what follows, it should be noted that all dicyanamide-perovskites exhibit only the μ₁,₅ (or μ₂ – η¹:η⁰:η¹) coordination mode, which is also the most common mode found in most dicyanamide-containing compounds [134].

Another remarked feature of the dca coordination modes is the bonding direction. In the literature, the μ₁,₅-dca coordination is generally represented as frontal bonding between the dca and the linked metals (Fig. 3) [134]. However, a deeper structural analysis (from the reported single crystal structures) shows that dicyanamide-perovskites present lateral dca-metal bonds related to the structural distortions (discussed further in section 3.3). In order to differentiate the observed lateral dca-metal bonds, we adapt the nomenclature reported for formate-perovskites [42], which identifies two types of bonding for each N-cyanide atom: *anti* and *syn* (Fig. 3). We define these bonding modes by studying the angle formed between the coordinated metal atom, the N-cyanide coordinating atom, and the N-amide non-coordinating atom (M−N−N). Accordingly, when the M−N−N angle is smaller
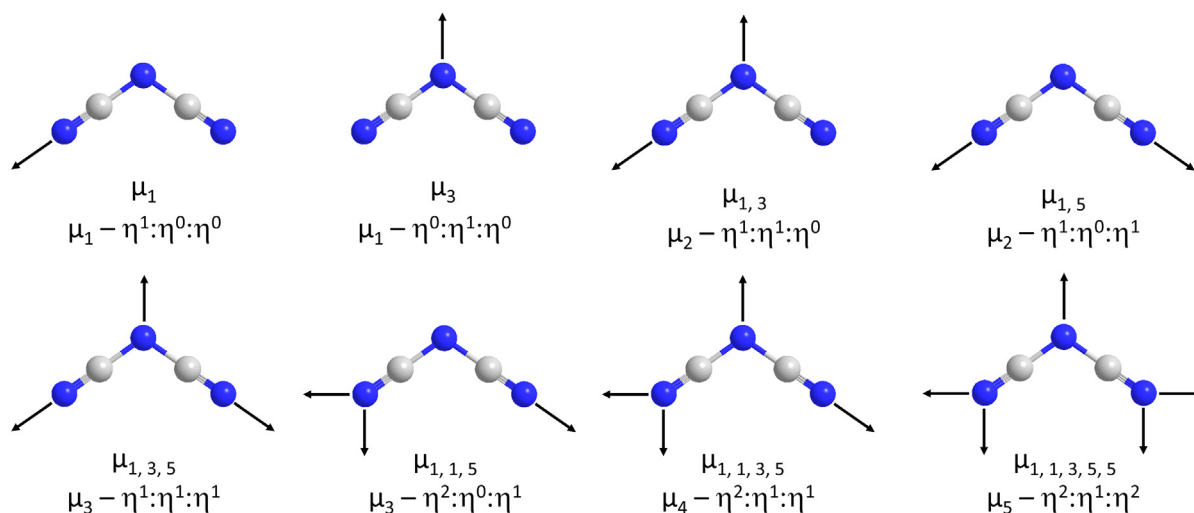
Fig. 2. Coordination modes of the conjugated dca ([N≡C-N-C≡N]⁻) ligand observed to date. The first nomenclature is the traditional short one (most commonly used in the literature), and the second nomenclature follows the normative IUPAC recommendations. Note: N-atoms are represented in blue, and C-atoms in grey.
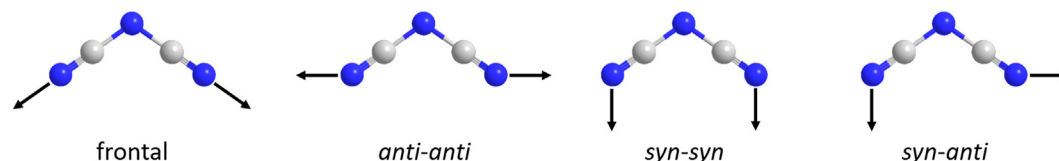
Fig. 3. $\mu_{1,5}$-dca bond directions, namely frontal bond and lateral (*anti-anti*, *syn-syn* and *syn-anti*) bonds. Note: N-atoms are represented in blue, and C-atoms in grey.

than π, the bond direction is syn. Meanwhile, when this angle is larger than π, the bond direction is considered *anti*. From the different combinations of the bonding directions of both terminal N-atoms, we identify three different possibilities: *anti-anti*, *syn-syn*, and *syn-anti* (Fig. 3).

In the ABX₃ dicyanamide-perovskites, these versatile dca anions occupy the X-site bridging divalent transition metal B cations (thus far only including Mn²⁺, Fe²⁺, Co²⁺, Ni²⁺ and Cd²⁺) and form [B (dca)₆] octahedra. Remarkably, these dca ligands, with lengths of ∼ 8.3 Å, are one of the longest ligands introduced to the HOIPs X-site (see Fig. 4). The resultant pseudo-cubooctahedral cavities are relatively large, which consequently allows the allocation of voluminous organic cations in the A-site (Fig. 5).

At the time of writing, there are around 32 compounds described that belong to this [A][B(dca)₃] family [73–85]. To further investigate their structural and chemical aspects, we have calculated the volume for all the A-cations reported for each one of the HOIPs families, using the reported crystallographic data and applying the promolecule surface method in the Crystal Explorer software (methodology explained further in the following section) [137,138]. The results are summarized in Fig. 6. As may be observed, dicyanamide-perovskites display the largest range of A-cation sizes, which can be attributed to the extraordinary length of the ligand and its ability to distort the structure (see section 3.3). This HOIP family can accommodate cations with sizes in the range of V = [207–374] Å (which represents up to 80% of size difference). Only a single reported example of dicyanometallate-perovskites [95,96], with formula [(Ph₃P)₂N][M(Au(CN)₂)₃] (M = Mn²⁺, Ni²⁺, Cd²⁺), contains a bigger A-cation than dicyanamide-perovskites. Even more interesting is the chemical diversity of these A-cations. In general, most HOIPs allocate only protonated alkylamines in the A-site. However, dicyanamide-perovskites can host a wide variety of A-cations, including alkylamoniums [73,75,77,79–81,84], alkylphosphoniums [76,82,83,85], alkylsulfoniums [74] and even organometallic cations [78], such as decamethylferrocenium or decamethylcobaltocenium.

All these factors identify the dicyanamide-perovskite family as one of the chemically and structurally richer compounds within HOIPs. Additionally, they also display a vast number of structural distortions and physico-chemical properties (some of them unique to this family) as discussed in the following sections.

3.2. Tolerance factor

Given the large number of possible combinations that may be used to form the ABX₃ structure of dicyanamide-perovskites, the tolerance factor (α) is a very useful tool to predict which of those combinations will result in the desired structure and accelerate materials discovery. This concept was first introduced by V. M. Goldschmidt in 1926 as a geometrical parameter for inorganic perovskites that relates the size of the cations in the A- and B-sites to that of the anions in the X-site, through Eq. (1): [2]

$$\alpha = \frac{r_A + r_X}{\sqrt{2}(r_B + r_X)} \tag{1}$$

In this model, the involved inorganic ions are considered as hard spheres with ionic radii of r_A, r_B and r_X for the A-, B- and X-sites, respectively. This simple, but very effective, relationship can be used to easily predict the formation of inorganic perovskites from different combinations of A, B and X ions. For values of α = [0.8–1], it is found that the selected combination will have a high probability of forming a perovskite structure. This structure is expected to display a cubic symmetry for α = [0.9–1], while structural distortions - specifically the octahedra tiltings described
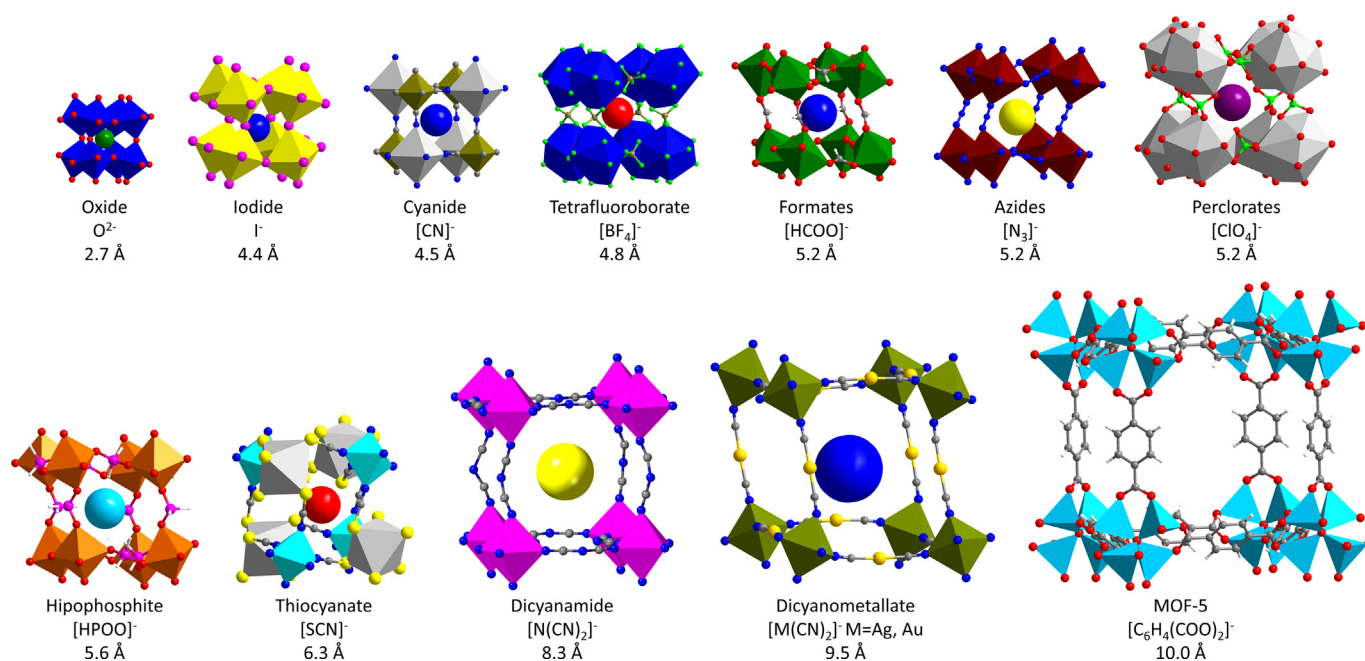
Fig. 4. Representation of general perovskite pseudo-cube for all the HOIPs with different X ligands, in comparison with the prototypical pseudo-cube of MOF-5, with their respective ligand's length indicated in Å.
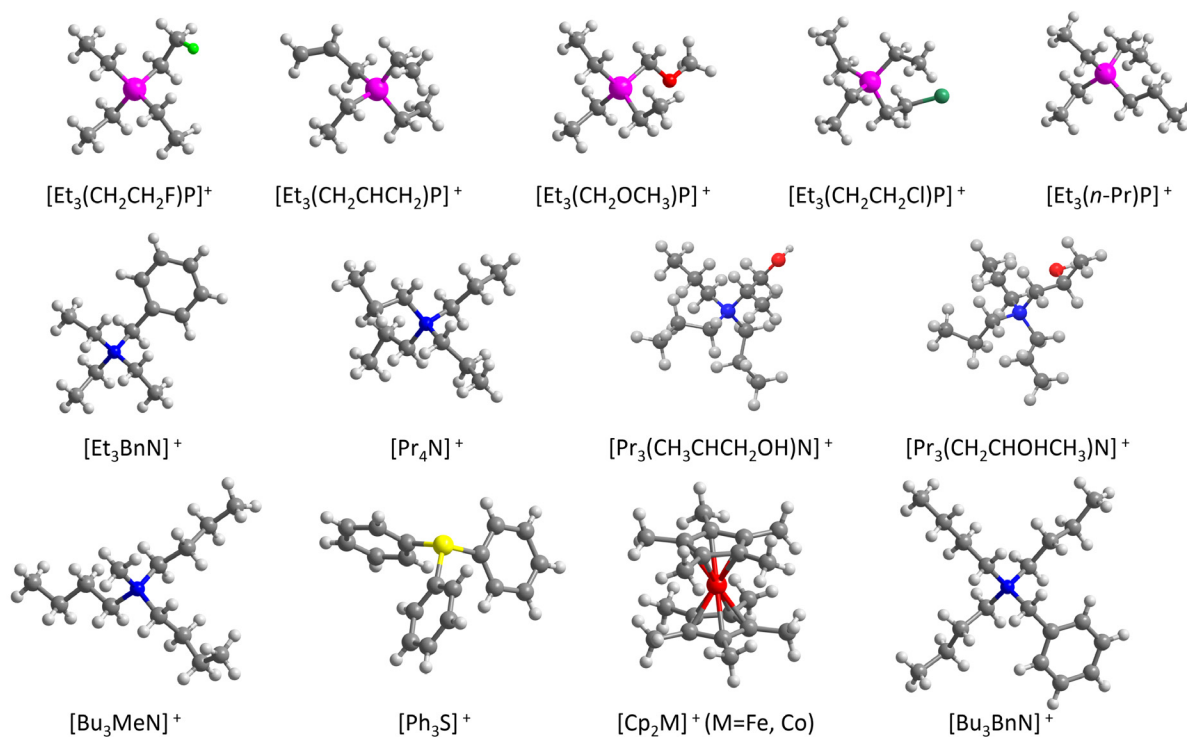
Fig. 5. Organic cations used in the A position of the reported [A][B(dca)$_3$] dicyanamide-perovskites [73–85].

by Glazer [139] - are expected for α = [0.8–0.89]. Tolerance factors outside this range will lead to different structural topologies, such as ilmenite (for α < 0.8) or hexagonal structures (α > 1).

In 2014, G. Kieslich, S. Sun and A. K. Cheetham extended the concept of the tolerance factor to HOIPs [140,141]. Here, new approaches are introduced which consider the irregular morphology of polyatomic A-cations and X-ligands. In this context, these authors assume rotational freedom of the organic A-cations around their centre of mass, which are considered as rigid spheres with an effective radii (r_{Aeff}) equivalent to:

$$r_{Aeff} = r_{mass} + r_{ion}$$

where r_{mass} is calculated using single crystal X-ray diffraction data as the distance between the centre of mass and the furthest atom
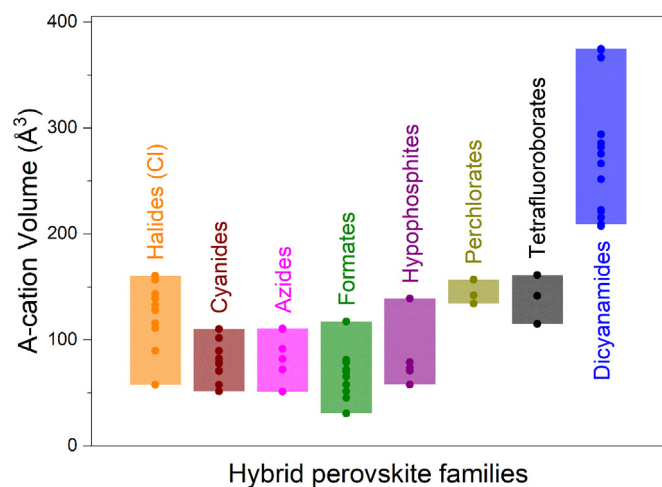
Fig. 6. Calculated volume of the A-site organic cations reported for each one of the HOIP families with X = chloride [18,169–173] (in representation of halide-perovskites), cyanide [56,59–61,63,64], azide [67,71,72], formate [39–46], hypophosphite [92,93], perchlorate [88–91], tetrafluoroborate (BF$_4$) [19,88] and dicyanamide [73–75,77,80,83–85]. Note: thiocyanate- [86,87] and dicyanometal-late-perovskites [95,96] are omitted as they allocate only one type of cation, namely, NH$_4^+$ (30.5 Å) and [(Ph$_3$P)$_2$N]$^+$ (595.3 Å), respectively. The volume of all A-cations has been calculated using the promolecule surface method in Crystal Explorer software [137,138].

from this centre (excluding hydrogen atoms), and r_{ion} is the corresponding ionic radii of this furthest atom [140,141].

In a similar way, X-anions are treated as rigid cylinders with effective radius (r_{Xeff}) and effective height (h_{Xeff}). All these new parameters are included in the revised Goldschmidt's tolerance factor for HOIPs, as indicated in equation (3):

$$\alpha = \frac{r_{Aeff} + r_{Xeff}}{\sqrt{2}(r_B + 0.5h_{Xeff})} \tag{3}$$

This extended concept also identifies a stability window of α = [0.8–1], where HOIP compounds with stoichiometry ABX$_3$ are expected to exhibit perovskite-like structures [140,141]. Using this model, G. Kieslich et al. were able to successfully explain and predict the stability of 180 halide perovskites and 562 HOIPs with "short" polyatomic X-anions, specifically, tetrahydroborate, formate, cyanide and azide anions [141]. However, to the best of our knowledge, only three works have addressed the tolerance factors of HOIPs with the largest X-anions, namely, dicyanamide and dicyanometallate ligands [81,84,96]. In these scarce works, dicyanamide-perovskites of general formula [PPN][M(Au(CN)$_2$)$_3$] (where PPN = [(C$_6$H$_5$)$_3$P)$_2$N]$^+$; M = Mn^{2+}, Ni^{2+}, Cd^{2+}) present a tolerance factor of α = [1.00–1.02], [96] and the dicyanamide-perovskites of general formula [Pr$_4$N][M(dca)$_3$] (where Pr$_4$-N = [(CH$_3$CH$_2$CH$_2$)$_4$N]$^+$, M = Mn^{2+}, Fe^{2+}, Co^{2+}, Ni^{2+}, Cd^{2+}; dca = [N(CN)$_2$]$^-$) show a factor of α = [1.00–1.04] [81,84].

For this review, we have followed the model proposed by G. Kieslich et al. to calculate the tolerance factors for all the reported dicyanamide perovskites [73–85], obtaining values of α = [0.95 – 1.30], with some of them somewhat higher that the expected α < 1. We suggest that this discrepancy is mainly related to the overestimation of the A-cations radii when considering them as rigid spheres, independently from their shape and anisotropy. This issue was recently addressed by M. Saliba et al. [142] who revised the tolerance factor for the [A][PbI$_3$] halide-perovskites with X = CH$_3$NH$_3^+$, (CH$_3$CH$_2$)NH$^+$, (NH$_2$)$_2$CH$^+$, (NH$_2$)$_3$CH, (CH$_3$CH$_2$)NH$_2^+$, (C$_3$H$_4$N$_2$)$^+$. In this work, the authors introduced the "molecular globularity" factor as $g = S/S_{eq}$. In this model, S is the actual molecular surface of the cation calculated by DFT methods, and S_{eq} is the surface of a sphere with a volume equal to the calculated molecular

Table 2
A-cation volume (V) and effective radii (r_{Aeff}) calculated using "promolecule electron density isosurface" methods [138], and tolerance factor (α) calculated for dicyanamide-perovskites with different A- and B-cations.

A-cation	V (Å³)	r_eff (Å)	B-cation	α	Crystallographic data ref.
[Et$_3$(CH$_2$CH$_2$F)P]$^+$	207.35	3.67	Mn^{2+}	0.85	[76]
			Cd^{2+}	0.83	[85]
[Et$_3$(CH$_2$CHCH$_2$)P]$^+$	208.8	3.68	Mn^{2+}	0.86	[83]
[Et$_3$(CH$_2$OCH$_3$)P]$^+$	215.18	3.72	Mn^{2+}	0.86	[83]
[Et$_3$(CH$_2$CH$_2$Cl)P]$^+$	221.11	3.75	Mn^{2+}	0.87	[76]
			Cd^{2+}	0.84	[85]
[Et$_3$(n-Pr)P]$^+$	222.41	3.76	Mn^{2+}	0.87	[83]
			Cd^{2+}	0.85	[82]
[Et$_3$BnN]$^+$	251.47	3.92	Mn^{2+}	0.89	[73]
			Fe^{2+}	0.9	[73]
[Pr$_4$N]$^+$	267.52	4	Mn^{2+}	0.9	[79,80]
			Fe^{2+}	0.91	[81]
			Co^{2+}	0.92	[81]
			Ni^{2+}	0.93	[79,81]
			Cd^{2+}	0.88	[84,127]
[Pr$_3$(CH$_3$CHCH$_2$OH)N]$^+$	275.34	4.04	Mn^{2+}	0.91	[77]
[Pr$_3$(CH$_2$CHOHCH$_3$)N]$^+$	281.57	4.07	Mn^{2+}	0.92	[77]
[Bu$_3$MeN]$^+$	285.58	4.09	Mn^{2+}	0.92	[75]
			Fe^{2+}	0.93	[75]
			Co^{2+}	0.94	[75]
			Ni^{2+}	0.95	[75]
[Ph$_3$S]$^+$	293.76	4.12	Mn^{2+}	0.92	[74]
[Cp$^*_2$Co]$^+$	366.2	4.44	Mn^{2+}	0.97	[78]
			Co^{2+}	0.99	[78]
			Ni^{2+}	1	[78]
[Cp$^*_2$Fe]$^+$	373.52	4.47	Mn^{2+}	0.98	[78]
			Fe^{2+}	0.99	[78]
			Co^{2+}	1	[78]
			Ni^{2+}	1.01	[78]
			Cd^{2+}	0.95	[78]
[Bu$_3$BnN]$^+$	374.35	4.47	Mn^{2+}	0.98	[73]
			Co^{2+}	1	[73]
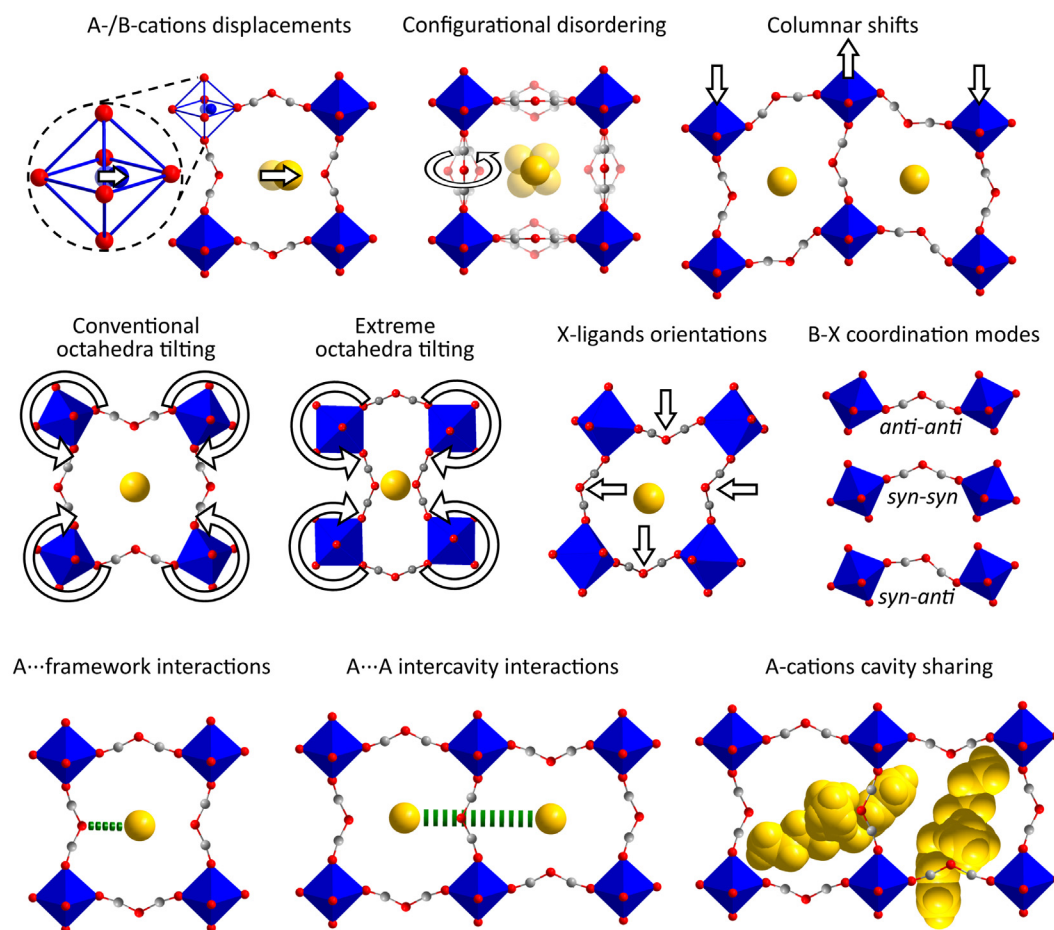
Fig. 7. Schematics of the different structural distortions found in dicyanamide-perovskites. Note: the represented octahedra tilting is conventional (neighboring octahedra rotate in opposite directions). In dicyanamide-perovskites non-conventional tilting (neighboring octahedra rotate in the same directions) is also possible. The represented columnar shifts are out-of-phase (displaced in opposite directions), although in-phase shifts (displacement in the same direction) is also possible. The represented X-ligands orientation is in-phase (dca ligands oriented in the same direction), although out-of-phase orientations are also possible (as represented in all the rest of archetypical perovskite-cubes of this figure).

volume [142]. They use this "molecular globularity" term to provide a linear correction for the tolerance factor, where they arbitrary consider $\alpha = 1$ for the [(NH$_2$)$_2$CH][PbI$_3$] pervoskite [142].

In this work, we propose a new and simpler method to obtain a more precise estimation for the A-cation radii. We use reported crystallographic data and the open access Crystal Explorer software [137] to calculate the A-cation volume enclosed by the "promolecule electron density isosurface" [138], a molecular surface that has been shown to be very similar to other *Ab initio* molecular surfaces but easier to calculate [137,138]. The obtained volume is approximated to a sphere that provides calculated ionic radii for the A-cations, as indicated in Table 2. When using these ionic radii in Equation (3), we obtain values of α = [0.83–1], which is now in full agreement with the stability window expected for perovskite-like structures. In comparison with the first method proposed to calculate tolerance factor in HOIPs [140,141], our new approximation can provide a more precise estimation of the A-cation size and, accordingly, of the α tolerance factor. In that regard, for example, the first method would have predicted that the family of [Bu$_3$MeN][M(dca)$_3$] do not display a perovskite-like structure due to an estimated tolerance factor of $\alpha \geq 1.2$. However, our method gives a more precise tolerance factor of $\alpha \leq 1$, which indicates that this family can display a perovskite-like structure, as experimentally demonstrated in the literature [75]. Therefore, our new approximation minimizes the risk of discarding possible HOIPs due to an overestimation of the A-cation size.

3.3. Structural distortions

The dicyanamide-perovskites display a large variety of structural distortions, which allows the framework to adapt to vast range of different sizes and shapes of the A-cations, as previously mentioned. In that regard, we have revisited the reported crystal structures of this family of HOIPs and have compiled their main structural distortions, which are summarized in Fig. 7 [143–145].

Some of these distortions are common to both inorganic perovskites and HOIPs (such as displacive, order–disorder and conventional octahedra tilting distortions). Meanwhile, some of them appear only in HOIPs with polyatomic X-ligands (such as non-conventional octahedra tilting, columnar shifts, different X-ligands orientations and B-X coordination modes, and interactions between the A-cation and the framework). Even more interestingly, a few of these distortions are exclusively found in dicyanamide-perovskites (such as what we have called "extreme octahedra tilting" or interactions between A-cations and cavity sharing, see detailed explanations below), with some of them being described and analysed for the first time in this review.

Starting with the first group, and similar to what is observed for some inorganic perovskites, almost all the reported dicyanamide-perovskites can exhibit displacive distortions that may imply the A- and/or B-cations, that is, off-centre shifts of these cations from the centre of the [AX$_{12}$] cuboctahedral cavities or the [BX$_6$]

octahedra, respectively. However, most of these displacements are antiparallel and/or randomly compensated so that they do not give rise to long-range ferroelectric order [80,81].

Another distortion, also frequently found in inorganic and HOIPs, is the configurational disordering of the structure, which in the case of the dicyanamide-perovskites can simultaneously appear in the A-cations and X-ligands. Due to the larger number of contributing atoms that may increase the degrees of freedom of dicyanamide compounds, their resulting configurational disorder is much larger than in other perovskites. Additionally, this disorder highly increases with temperature and, in some cases, the dca ligands even act as rotors around the M−M longitudinal axis [80,81].

The so-called columnar shifts are relatively new structural distortions that have only been observed in HOIPs. This term was introduced by A. L. Goodwin *et al.* in 2016 as a new symmetry-breaking element in these materials. Columnar shifts refer to correlated displacements of columns of connected $[BX_6]$ octahedra $(...-[BX_5]-X-[BX_5]-...)$, which can be displaced out-of-phase (in antiparallel directions) or in–phase (in the same direction) [145]. In the literature, out-of-phase columnar shifts have already been reported [84,145], and are the most commonly observed displacements.

As for structural distortions derived from octahedral tiltings, it is best to first describe the concepts of conventional and non-conventional tiltings before explaining the recently observed "extreme octahedra tilting". In this context, the first term refers to the distortions in which neighbouring octahedra rotate in opposite directions (see Fig. 7) [139]. This is the situation typically found in perovskites with monoatomic X-anions (i.e. inorganic perovskites and hybrid halide perovskites) [139], which can exclusively exhibit this type of rotation. This distortion is also found in most dicyanamide-perovskites. In addition, HOIPs containing polyatomic ligands in the X-site may also present the so-called "forbidden" or non-conventional rotations, where neighbouring octahedra rotate in the same direction. However, these distortions are very rare and, up to now, were only found in a few perovskites, where X = azide [68,120,146], dicyanometallate [96], and hyphophosphite [92].

Traditionally, conventional tilting in oxide- and halide-perovskites can be described by the simple Glazer notation [139]. However, HOIPs show the coexistence of conventional and non-conventional tilts together with columnar shifts, which hinder the use of this simple notation to unambiguously defined tilting modes. Accordingly, HOIPs octahedral tilts are normally defined by using complex group-theoretical software, rigid unit modes

(RUMs) and the corresponding irreps, although these studies are still scarce. At this point, it should be noted that a complex "tilting engineering" study is far from the scope of this review, and the reader can find excellent works on this topic elsewhere [143–145]. In the same line, our investigation into the reported structures also helped us discover another rare form of octahedra tilting, where we found that the $[Et_3(CH_2CH_2F)P][Mn(dca)_3]$ perovskite (and its Cd-analogue [85]) exhibits a singularity never observed before in other HOIPs. We understand that, since $[Et_3(CH_2CH_2F)P]^+$ is the smallest A-cation fitted in a dicyanamide-perovskite [76,85], the framework has to largely shrink the A-cavities to accommodate this. The framework consequently rotates the octahedra in a peculiar and unprecedented form of tilting, which we have named "extreme octahedra tilting". This distortion consists of conventional tilts with a maximized angle of rotation of 45°, where the octahedra edges adopt a face-to-face orientation (Fig. 8). Following this strategy, the cavity of this perovskite achieves a volume reduction of ∼ 80 % in comparison with the dicyanamide–perovskite that integrates the largest A-cation so far, namely, the $[Bu_3BnN]^+$ cation [73].

In order to illustrate the diversity of distortions that the dicyanamide-perovskites can exhibit, we have chosen three compounds as case studies (Fig. 9). The first one is $[Pr_4N][Fe(dca)_3]$ [81] (polymorph observed at 200 K), which shows out–of–phase columnar shifts along the *a*- and *b*-axes with conventional octahedra tilts perpendicular to the *ab*-plane (red arrows), which results in an out-of-phase orientation of the dca-ligands along the *a*- and *b*-axis (green arrows). The second compound, $[Et_3(CH_2CH_2F)P][Mn(dca)_3]$ (polymoprh observed at 293 K) [76], exhibits in-phase columnar shifts along the [0 1 1] direction and conventional octahedral tilting perpendicular to the (1 1 $\bar{1}$) plane (red arrows), which leads to an out-of-phase orientation of the dca ligands along the [0 2 0] and [1 $\bar{2}$ 2] directions (green arrows). Finally, the $[Et_3(CH_2OCH_3)P][Mn(dca)_3]$ [83] (200 K polymorph) shows in-phase columnar shifts along the *c*-axis and non–conventional octahedral tilting perpendicular to the *ac*-plane (red arrows), resulting in the dca ligands being oriented in-phase along the *c*-axis and along the [3 $\bar{1}$ 2] direction (green arrows).

We can therefore deduce that the combination of the columnar shifts and the octahedra tilting influences the orientation of the dca ligand when coordinated in the framework. In that regard, conventional octahedra tilting, together with in-phase or out-of-phase columnar shifts, give rise to dca ligands oriented out-of-phase. Meanwhile, non-conventional octahedra tilting together with in-phase columnar shifts induces in-phase orientation of dca ligands. Furthermore, these distortions highly affect the size and shape of

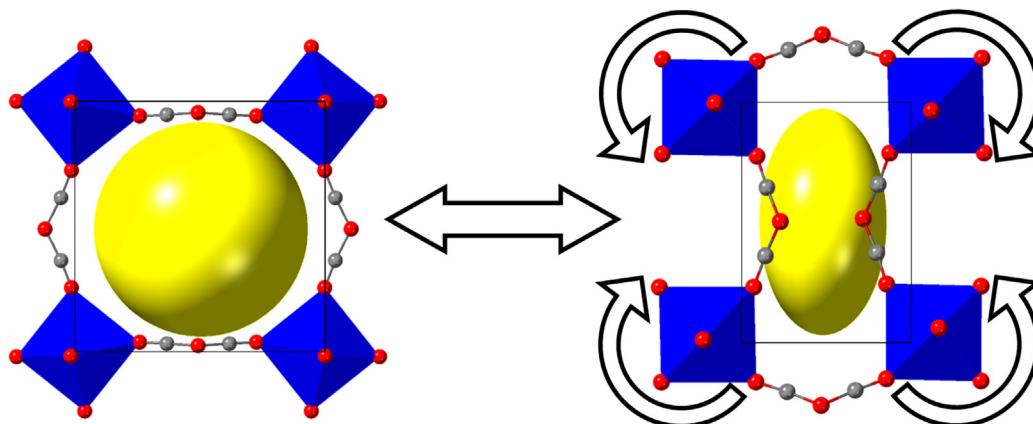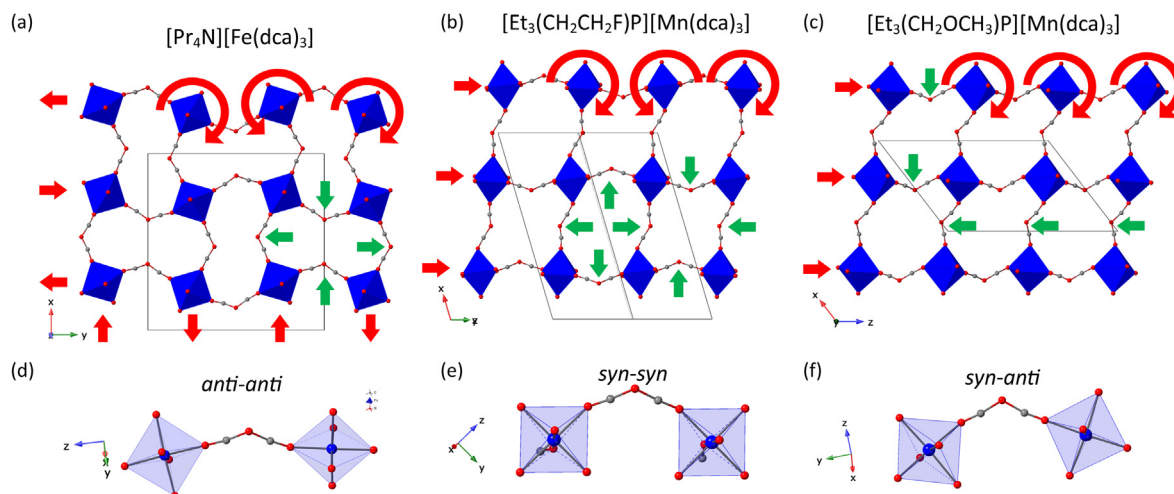**Fig. 8.** Schematics of the "extreme octahedral tilting" observed in the dicyanamide-perovskites $[Et_3(CH_2CH_2F)P][M(dca)_3]$ (M = Mn^{2+}, Cd^{2+}) [76,85], where the octahedra exhibit a conventional rotation with a maximized angle of 45° facing edges.

Fig. 9. Selected structural distortions for the (a,d) [Pr₄N][Fe(dca)₃] [81] (b,e) [Et₃(CH₂CH₂F)P][Mn(dca)₃] [76], and (c,f) [Et₃(CH₂OCH₃)P][Mn(dca)₃] [83] dicyanamide-perovskites. Note: straight red arrows represent columnar shifts, curved red arrows represent octahedral tilting, and straight green arrows represent X-ligands orientations. Unit-cells are represented by black lines.

the cavities and their windows. For instance, the [Pr₄N][Fe(dca)₃] shows double-pentagon cavity-windows, the [Et₃(CH₂CH₂F)P][Mn (dca)₃] displays both star-shaped and oval-shaped cavity-windows, and the [Et₃(CH₂OCH₃)P][Mn(dca)₃] compound exhibits a mushroom-shaped cavity-window (see Fig. 9a-c).

It should be noted that this is the first time that non-conventional octahedra tilting and in-phase columnar shifts have been identified and described for dicyanamide-perovskites, further enlarging the already rich diversity of distortions known for this family of compounds.

These three compounds can also serve as an example for the different B-X coordination modes depending on the M−N−N angle. As was explained in section 3.1, when the internal M−N−N angle of dca is bigger than π, we denote the coordination as an *anti* mode. On the contrary, when this angle is smaller than π, the coordination is called a *syn* mode. As the dca ligand has two N-amide coordinating centres, there are three possible coordination modes:

anti-anti, *syn-syn* and *syn-anti* (see Fig. 3 and 9d-f). The *anti-anti* and *syn-anti* modes have already been observed in formate-perovskites [42], however here we identify a *syn-syn* coordination mode in the [Et₃(CH₂CH₂F)P][Mn(dca)₃] perovskite that, to the best of our knowledge, is described for the first time in any member of the vast HOIP family.

Following more complex distortions, and as already mentioned in the case of "extreme octahedra tilting", the dicyanamide-perovskites use distortions as a strategy to accommodate A-cations. For example, we understand that for accommodating cations as large as [Bu₃BnN]⁺, [Et₃BnN]⁺ or [Ph₃S]⁺ [73,74], the dicyanamide-perovskites find a solution unobserved in any other HOIP, and that more closely resemble characteristics typical of MOFs. In this case, the large A-cations can partially occupy more than one [AX₁₂] cavity and, on the other side, there is a "cavity sharing" where each [AX₁₂] cavity hosts two partial A-cations (see Fig. 10).
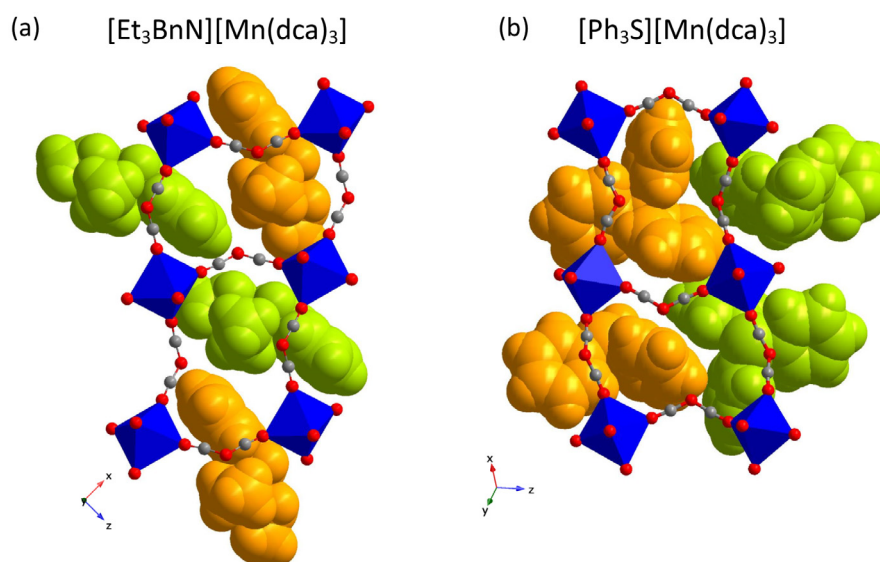
Fig. 10. Examples of the cavity sharing of A-cations inside the same [AX₁₂] cuboctahedron for the (a) [Et₃BnN][M(dca)₃] (M = Mn²⁺, Fe²⁺) [73] and (b) [Ph₃S][Mn(dca)₃] [74] perovskites. Note: A-cations sharing the same cavity are represented by different colours (green and orange) to aid visualization.

(a) $[Et_3(CH_2CH_2Cl)P][Mn(dca)_3]$ (b) $[Et_3BnN][Mn(dca)_3]$
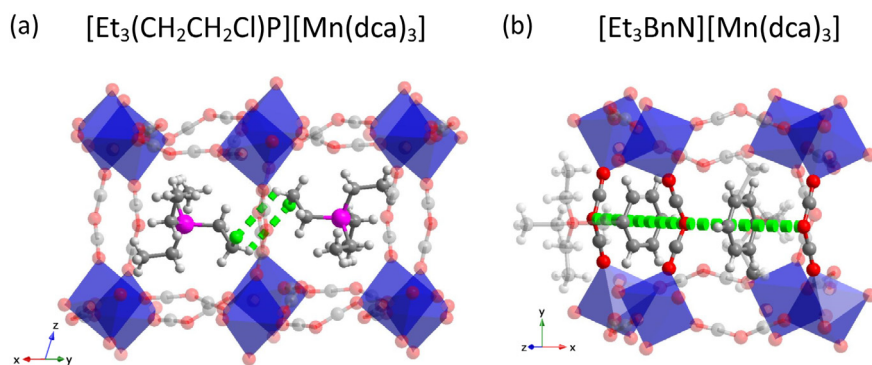
Fig. 11. (a) Intercavity interactions of "AH···XA" hydrogen bonds observed in $[Et_3(CH_2CH_2Cl)P][M(dca)_3]$ (M = Mn^{2+} and Cd^{2+}) perovskites [76,85], and (b) detected supramolecular $\pi\cdots\pi$ staking interactions between the benzyl groups of the A-cations and dca-ligands of the framework in $[Et_3BnN][M(dca)_3]$ (M = Mn^{2+}, Fe^{2+}) [73] perovskites. Note: transparent colours are used to aid visualization of the interacting parts represented by solid colours. Green dash lines are visual guides representing the interactions.

In addition, dicyanamide-perovskites can also exhibit interactions between the A-cations and the framework. Some of these interactions, such as the "A-H···X" hydrogen bonds first reported by M.-L. Tong *et al.* in dicyanamide-perovskites [73], are also observed in other HOIPs [53]. However, the large volume of the cuboctahedra cavities allows the presence of new supramolecular "A···A" and "A···framework" interactions, which are uncommon in HOIPs but generally found in MOFs. For instance, our deep structural study for this review reveals "intercavity interactions" of A-cations through "A–H···Cl-A" hydrogen bonds. This phenomena occurs in the $[Et_3(CH_2CH_2Cl)P][M(dca)_3]$ (M = Mn^{2+} and Cd^{2+}) perovskites [76,85], see Fig. 11**a**.

In addition, we also notice the presence of singular "$\pi\cdots\pi$" staking interactions between the dca-ligands and the aromatic rings of A-site cations, which occurs in $[Et_3BnN][M(dca)_3]$ (M = Mn^{2+}, Fe^{2+}) and $[Bu_3BnN][M(dca)_3]$ (M = Mn^{2+}, Co^{2+}) (Fig. 11**b**). In view of these uncommon features, we anticipate that such intermolecular interactions could give rise to new functional properties, such as charge transport or photosensitivity.

4. Stimuli responsive properties and applications

4.1. Mechanical properties

The broad sub-division of the coordination polymer family into those which are porous (i.e. MOFs) and those which are dense (including HOIPs), relies on the size of pores and their capacity to absorb/desorb guest molecules [101,102,104–106]. The extent of this porosity is also correlated to their physical properties such as density, hardness and Young's modulus. For example, Fig. 12 shows the unit cell volume normalized per Z (V_{cell} / Z) versus density (ρ) for reported ABX_3 HOIPs in comparison with selected oxide-perovskites and MOFs.

The much larger distribution of density and unit cell volumes for MOFs is credited to their rich diversity of organic ligands (where larger ligands normally lead to larger unit cell volumes), and the possibility of guest molecule incorporation (MOFs containing guest molecules are generally denser than those without them). On the other hand, oxide-perovskites show lower unit cell volumes (V_{cell} / Z = [55–73] $Å^3$) and the largest densities (ρ = [4–7] g cm^{-3}) due to their compactness and the presence of only inorganic ions in their structure. Halide-perovskites exhibit a narrow distribution of unit cell volumes (V_{cell} / Z = [189–390] $Å^3$) though density values can show large differences (ρ = [1.6–4.3] g cm^{-3}) depending on whether the structure contains heavy-metals (i.e.

Pb or Sn) or not. Most of the remaining HOIPs are distributed in a central core-region with values ranging in V_{cell} / Z = [178–500] $Å^3$ and ρ = [1.3–2.7] g cm^{-3}.

The dicyanometallates are one notable exception, showing larger unit cell volumes due to their long X-ligands. Such long 'X' ligands also bestow the dicyanamide-perovskites with larger unit cell volumes than the bulk of the perovskite family and provide them with their intermediate position on the Ashby plot in Fig. 12.

The mechanical properties, and in particular Hardness, *H* and (average) Youngs's modulus, *E*, of both the wider perovskite family and MOFs have been extensively investigated. Several excellent reviews exist in the area [124,147,148]. An Ashby plot of selected data for some formiate-, azide-, halide-, hyphophosphite-, and dicyanamide-perovskites compared with selected oxide-perovskites (BaTiO$_3$ and CaTiO$_3$) and MOFs (ZIFs and MOF-5) [124,147] again reveals the position of the dicyanamides as intermediate between the 'soft' porous crystals indicative of MOFs [149], and the more dense inorganic and HOIP structures (Fig. 13). This is consistent with the correlation between both
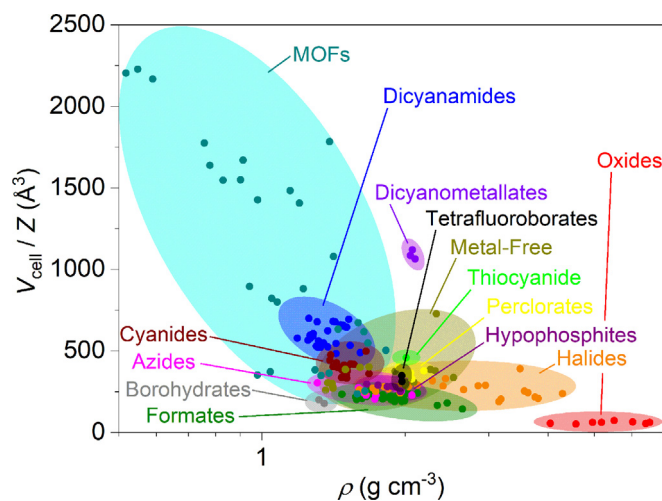
Fig. 12. Comparison of unit cell volume normalized per Z (V_{cell} / Z) and density (ρ) for reported ABX_3 HOIPs with X = halides [169,170,172–181], formate [23–27,29,31–36,38–53], hypophosphite [92,93], perchlorate [88–91,182], cyanide [55–64], thiocyanate [87], tetrafluoroborate [19,88], tetraborohydrate [94], azide [65–72], dicyanamide [73–85] and dicyanometallate [95,96] and selected metal-free perovskites [17–19], oxide-perovskites [183] and MOFs [103,184–192].
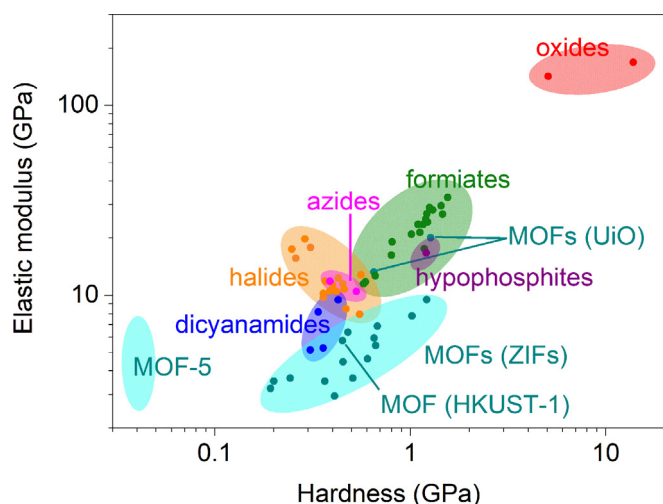
Fig. 13. Elastic modulus *versus* hardness of selected HOIPs and MOFs 0 [124,147,148,193,194]. Note: the dicyanamide-perovskites [Pr$_4$N][Mn(dca)$_3$] and [Pr$_4$N][Cd(dca)$_3$] show elastic moduli of 6.2 GPa and 8.1 GPa, respectively [125,127], but they are not included in the graphic because hardness have not been yet reported for these materials. Likewise, the MOF UiO-66 shows an elastic modulus of 28 GPa [195,196].

the resistance to uniaxial deformation (*H*) and mechanical compliance (*E*).

4.2. Thermal properties

4.2.1. Thermal decomposition

Recent studies on the thermal stability of [Pr$_4$N][M(dca)$_3$] (M = Mn^{2+}, Fe^{2+}, Co^{2+}, Ni^{2+}) have shown that these compounds remain stable up to $\sim$ [513–554] K (Table 3) [131,132]. Above those temperatures, the Ni- and Co-perovskites display a structural transformation into M(dca)$_2$ (M = Ni^{2+}, Co^{2+}) and a further thermal decomposition that liberates [Pr$_4$N]$^+$ cations and part of the dca anions [132]. The temperature at which the [Pr$_4$N]$^+$ cations are released is relatively similar to the temperature at which MOFs liberate coordinating guest molecules (T $\sim$ [373–473] K) [150]. However, while MOFs may maintain their structural integrity after molecules release (in some cases up to T > 773 K) [150–152], the

structures of dicyanamide-perovskite change and/or collapse during A-cation liberation, given the absence of framework stabilizing electrostatic interactions. Subsequent studies on [Et$_3$(CH$_2$CH$_2$X)P] [Mn(dca)$_3$] (X = F$^-$, Cl$^-$) [85,76] have shown that these compounds present larger thermal stabilities of $\sim$ 530 K and $\sim$ 588 K, respectively. Meanwhile, [Et$_3$(*n*-Pr)P][Cd(dca)$_3$] [82] is stable up to 550 K. These temperatures should however be taken as a guide and not as absolute values, as T_{dec} is very sensitive to analysis conditions (such as heating rate, atmosphere, or even sample amount).

Similar to their porous hybrid relatives, the controlled thermal decomposition of dicyanamide-perovskites has been utilized as a precursor for porous carbon. It should first be noted that thermally-induced transformations of precursors into new materials normally leads to partial mass losse. J. M. Bermúdez-García *et al.* therefore proposed some modifications to the standard synthetic method used to obtain single-crystals of dicyanamide-perovskites [132]. Single crystals of these compounds are normally obtained by slow-evaporation from a few millilitres of water-alcohol solutions over the course of several days. The proposed modification consisted of using hundreds of millilitres of the starting solutions and accelerating the evaporation using rotatory evaporation [132]. This method produced the desired compounds as polycrystalline powders (rather than single-crystals) on a larger scale of over 55 g (compared to a few mg) with 95% yield, and within a few minutes of evaporation (instead of several days) [132]. This method therefore accelerates the reaction and provides larger quantities of the starting dicyanamide-perovskites as precursor for other derived materials (see Fig. 14a).

The [Pr$_4$N][M(dca)$_3$] (M = Co^{2+}, Ni^{2+}) compounds were found to act as precursors for nitrogen-enriched carbon nanotubes with embedded magnetic nanoparticles M@CNTs (M = Co, Ni) (see Fig. 14c-d). These materials could be obtained in relatively large quantities (over 5 g, Fig. 14b) by simple thermal treatment at medium-temperatures of 1200 K under a nitrogen atmosphere. The resultant M@CNTs were shown to selectively absorb spilled oil from water ($\sim$2.2 g g^{-1}) and could be easily recovered from the liquid using a magnet, which is useful for pollutants recovery [132].

4.2.2. Melting and glass formation

Several examples of dca-perovskites have been found to show solid–liquid melting transitions prior to thermal decomposition.
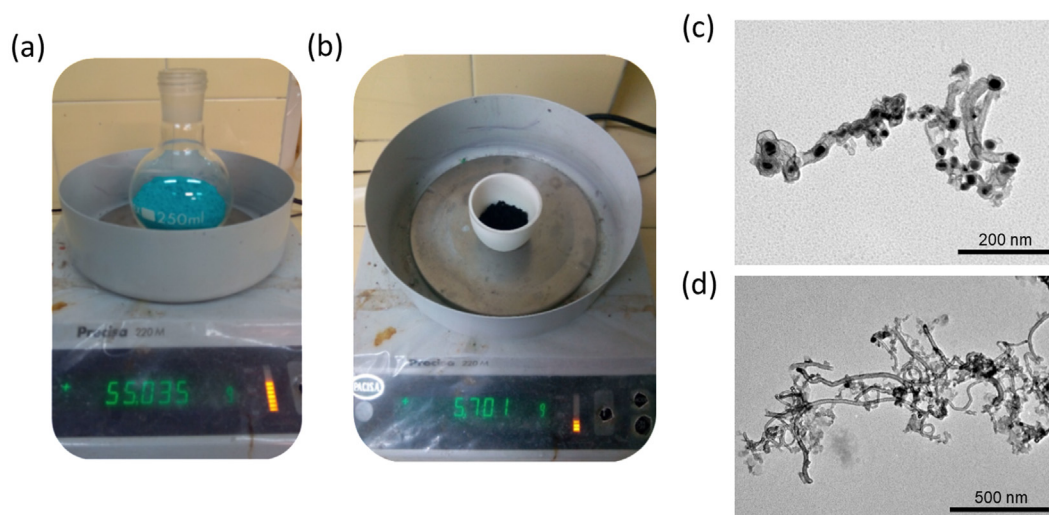
Fig. 14. Optical images of (a) the scaled-up [Pr$_4$N][Ni(dca)$_3$] perovskite using fast-evaporation methods and the (b) Ni@CNTs derived material from calcination at 1200 K, and TEM micrographs of the (c) Ni@CNTs and (d) Co@CNTs samples obtained after annealing at 900 °C ($\sim$1200 K). Figures adapted with permission from reference [132].

Table 3

Selected thermodynamic parameters of the reported dicyanamide-perovskites. Note: T_t = transition temperature, ΔH = transition enthalpy change, ΔS = transition entropy change, T_h = transition temperature on heating, T_c = transition temperature on cooling, $T_{melt.}$ = melting temperature, $T_{cryst.}$ = crystallization temperature, $T_{dec.}$ = decomposition temperature.

Perovskite	Structural transition	T_t (K)	ΔH (kJ kg^{-1})	ΔS (J K^{-1} kg^{-1})	T_h - T_c (K)	T_{melt} (K)	T_{cryst} (K)	T_{dec} (K)	Ref.
[Pr$_4$N][Mn(dca)$_3$]	P $\overline{4}$ 2$_1$c → I4/mcm	332	12.7	38.2	3	544	–	554	[79,80,130,131]
[Pr$_4$N][Fe(dca)$_3$]	P $\overline{4}$ 2$_1$c → Pnna	286	4.8	16.6	7	536	–	546	[81,131]
	Pnna → Ibam	300	2.9	9.5	8				
	Ibam → I4/mcm	331	5.3	16.1	1				
[Pr$_4$N][Co(dca)$_3$]	P $\overline{4}$ 2$_1$c → Pnna	246	4.0	16.5	16	503	–	540	[81,131,132]
	Pnna → Ibam	301	3.0	10.1	9				
	Ibam → I4/mcm	341	4.8	14.0	2				
[Pr$_4$N][Ni(dca)$_3$]	P $\overline{4}$ 2$_1$c → Pnna	216	0.8	3.8	41	–	–	523	[81,132]
	Pnna → Ibam	302	2.7	8.8	11				
	Ibam → I4/mcm	356	4.5	12.6	1				
[Pr$_4$N][Cd(dca)$_3$]	P2$_1$/n → -	228	2.9	13.1	–	–	–	513	[84,127]
	- → P $\overline{4}$ 2$_1$c	242	1.2	5.0	4				
	P $\overline{4}$ 2$_1$c → Ibam	363	0.3	0.8	3				
	Ibam → I4/mcm	387	5.7	14.9	3				
[Bu$_3$MeN][Mn(dca)$_3$]	P2$_1$/n → Pnma	384	11.5	30.2	Non-rever.	404	[387–397]	–	[75]
[Bu$_3$MeN][Fe(dca)$_3$]	P2$_1$/n → -	399	24.5	61.1	29	409	–	–	
[Bu$_3$MeN][Co(dca)$_3$]	P2$_1$/n	–	–	–	–	389	[344–353]	–	
[Bu$_3$MeN][Ni(dca)$_3$]	P2$_1$/n → -	394	26.5	67.3	48	434	–	–	
[Et$_3$(CH$_2$CH$_2$F)P][Mn(dca)$_3$]	C2/c → Pnca	332	33.7	101.4	∼ 43	–	–	530	[76]
	Pnca → I4$_1$/acd	411	0.6	1.4	∼ 6				
[Et$_3$(CH$_2$CH$_2$Cl)P][Mn(dca)$_3$]	P2$_1$/c → Pbcn	300	33.3	111	∼ 19	–	–	588	
	Pbcn → P4/mmm	399	1.1	2.8	∼ 6				
[Et$_3$(CH$_2$CH$_2$F)P][Cd(dca)$_3$]	C2/c → Cmca	357	–	–	∼ 48	–	–	–	[85]
	Cmca → P4$_2$/nnm	428	–	–	∼ 10				
[Et$_3$(CH$_2$CH$_2$Cl)P][Cd(dca)$_3$]	P2$_1$2$_1$2$_1$ → Pbcn	320	–	–	∼ 40	–	–	–	
	Pbcn → I4$_1$/adc	374	–	–	∼ 20				
[Et$_3$(CH$_2$CHCH$_2$)P][Mn(dca)$_3$]	P2$_1$/c → I4/mcm	350	11.9	33.7	10.8	–	–	–	[83]
[Et$_3$(CH$_2$OCH$_3$)P][Mn(dca)$_3$]	P2$_1$/c → P2$_1$2$_1$2$_1$	265	–	–	21.2	–	–	–	
	P2$_1$2$_1$2$_1$ → I4$_1$/amd	333	23.0	69.5	14.5				
[Et$_3$(n-Pr)P][Mn(dca)$_3$]	P2$_1$2$_1$2$_1$ → I4/mcm	363	26.4	72.6	10.1	–	–	–	
[Et$_3$(n-Pr)P][Cd(dca)$_3$]	P2$_1$/c → P2$_1$2$_1$2$_1$	270	6.9	25.6	12	–	–	550	[82]
	P2$_1$2$_1$2$_1$ → Ibam	386	18.1	46.9	7				
	Ibam → Cmca	415	0.3	0.7	4				
[Pr$_3$(CH$_2$CHOHCH$_3$)N][Mn(dca)$_3$]	P $\overline{4}$ 2$_1$c → I4/mcm	207	–	–	12.5	–	–	506	[77]
[Pr$_3$(CH$_3$CHCH$_2$OH)N][Mn(dca)$_3$]	Pna2$_1$ → P2$_1$2$_1$2$_1$	267	4.1	15.3	18	–	–	499	
	P2$_1$2$_1$2$_1$ → Pnam	287	1.1	3.9	5.7				
	Pnam → I4/mcm	331	8.6	26.1	28.9				

Such instances arise due to rare events of M−N coordination bond breakage at high temperature, and result in a liquid state of largely unknown structure. In one example, Shaw *et al.* demonstrated that compounds of formula [Pr$_4$N][M(dca)$_3$] (M = Mn^{2+}, Fe^{2+}, Co^{2+}) [131] undergo melting at 544, 536 and 503 K respectively. This trend may be explained by the polarizing power of the M species, with those more polarizing resulting in more covalent M−N bonds which break at lower temperatures. The free energy barrier to melting in the case of [Pr$_4$N][Mn(dca)$_3$] has been calculated as 85 kJ mol^{-1}. Mączka *et al.* have also noted melting in the [Bu$_3$-MeN][M(dca)$_3$] (M = Mn^{2+}, Fe^{2+}, Co^{2+}, Ni^{2+}) [75] series of compounds (Table 3). Such values compare favourably with those of several MOF structures reported to melt (583 K, 701 K, 710 K, 740 K and 866 K) [153–155]. It is surprising, given the interest in the dicyanamide family, that such results are very recent – though it is clear that further work on both the characterization of the liquid state and the accurate delineation of decomposition/melting processes, is warranted.

Quenching of a liquid phase at sufficiently high cooling rates to avoid crystallisation remains the most common method of glass formation [156]. The formation of glasses has been demonstrated from several MOFs, with the resultant hybrid species being assigned to a new, 4th category of melt quenched glass [157], in addition to inorganic, metallic and organic. Here however, it is metastable, porous frameworks which are quenched into more dense glasses. This consequently means that the absence of recrystallisation upon cooling, or reheating is to be expected, given the absence of any thermodynamic driving force to create an open framework from a dense material.

Mączka *et al.* demonstrated the absence of decomposition or immediate recrystallisation in [Bu$_3$MeN][M(dca)$_3$] species upon melt-quenching, though suggested, based on acquired Raman data, that slow recrystallisation could not be ruled out [75]. Shaw *et al.* then reported that even relatively slow cooling rates resulted in glass formation from [Pr$_4$N][M(dca)$_3$] melts [131]. Pair distribution function analysis, alongside both solid-state nuclear magnetic resonance (NMR) spectroscopy, and high resolution mass spectrometry were carried out on the quenched glass species. These confirmed the presence of Pr$_4$N, dca and M species, though magnetic characterization data indicated the partial reduction of the M species upon melting [131].

4.2.3. Solid-state transformations

At lower temperatures, most dicyanamide-perovskites exhibit thermally-induced reversible structural transitions (Table 3), involving order–disorder processes of the dca ligands and/or A-cations, out-of-center displacements of the A-cations and changes in the columnar shifts [80,81,84,144]. Some of these materials exhibit a single phase transition, while others can display multiple (up to four) transitions. Preliminary results suggested that this difference could be related to the B-cation radii and the tolerance factor of the given dicyanamide-perovskite [80,81,84]. In the [Pr$_4$N][M(dca)$_3$] (M = Mn^{2+}, Fe^{2+}, Co^{2+}, Ni^{2+}, Cd^{2+}) family, the Mn-compound exhibits only one phase transition, compared to structural
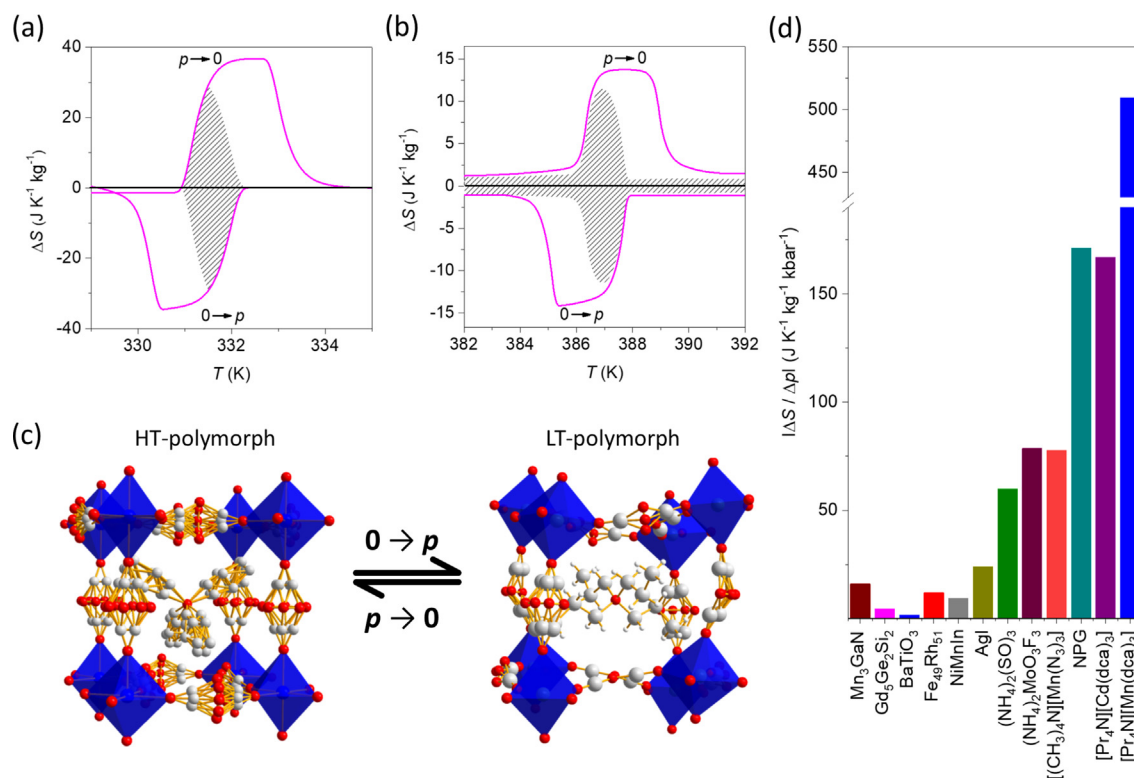
Fig. 15. Barocaloric effects in terms of isothermal entropy change, ΔS, for the (a) $[Pr_4N][Mn(dca)_3]$ and (b) $[Pr_4N][Cd(dca)_3]$ compounds induced under pressures of $p = 68.9$ bar. Figures adapted with permission from references [84,130]. (c) HT- and LT-polymorphs involved in the pressure-induced barocaloric effects of $[Pr_4N][Mn(dca)_3]$. (d) Comparison of the barocaloric strength, $\Delta S/\Delta p$, for different barocaloric materials. Note: NiMnIn refers to the alloy of stoichiometry $Ni_{49.26}Mn_{36.08}In_{14.66}$ and NPG refers to the neopenthylglicol $((CH_3)_2C(CH_2OH)_2)$ plastic crystal.
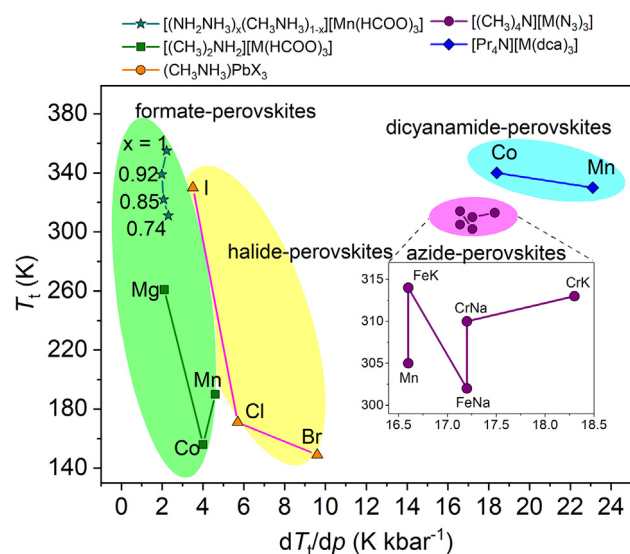
Fig. 16. Ashby plot of selected barocaloric parameters of transition temperature, T_t, and barocaloric coefficient, dT_t/dp, for different HOIPs. Figures adapted with permission from reference [161].

analogues with B-cations of smaller (Fe^{2+}, Ni^{2+}, Co^{2+}) and larger (Cd^{2+}) ionic radii, which display multiple transitions [80,81,84]. Therefore, within this family of compounds, it is assumed that $[Pr_4N][Mn(dca)_3]$ exhibits a tolerance factor closer to "ideal", resulting in less structural strain and, consequently, fewer structural transitions. However, this tendency is not observed in other

dicyanamide-perovskite families (see Tables 2 and 3), which suggest that other parameters (intermolecular interactions, for instance) might have a more prominent role.

4.3. Response to pressure

Regarding the pressure-responsiveness of this family of materials, J. M. Bermúdez-García et al. found that the transition temperatures of the $[Pr_4N][M(dca)_3]$ (M = Mn^{2+}, Fe^{2+}, Co^{2+}, Ni^{2+}, Cd^{2+}) perovskites can be shifted by applying external pressures of extremely low magnitude [80,81,84,130] These findings highlighted the potential of HOIPs as a new family materials with giant barocaloric effects. Giant barocaloric effects are defined as large thermal changes (isothermal entropy changes, $\Delta S > 10$ J K^{-1} kg^{-1}, or adiabatic temperature changes, $\Delta T > 5$ K) induced by the application of external hydrostatic pressure [158]. Contrary to most barocaloric materials (which require operating pressures over 1000 bar), the dicyanamide-perovskites exhibit giant barocaloric effects (of up to $\Delta S = 37.0$ J K^{-1} kg^{-1}) under pressures below 70 bar (Fig. 15) [130]. This unprecedented response towards pressure is related to the extremely large flexibility of those dicyanamide-perovskites, which show values of $dT_t/dp = 23.1$ K kbar^{-1} in the case of the Mn-compound and $dT_t/dp = 38.2$ K kbar^{-1} for the Cd-analogue [84,130]. Therefore, dicyanamide compounds exhibit the largest barocaloric strength (i.e. barocaloric effect normalized by applied pressure, $\Delta S/\Delta p$) reported in the literature [84,130], even larger than in the case of the recently discovered barocaloric plastic crystal [159,160].

Later studies by M. Mączka et al. deepened in the relationships between the crystal structure and the large pressure responsiveness by using variable-pressure XRD [125,127]. These studies revealed that the compressibility in $[Pr_4N][Mn(dca)_3]$ and $[Pr_4N]$
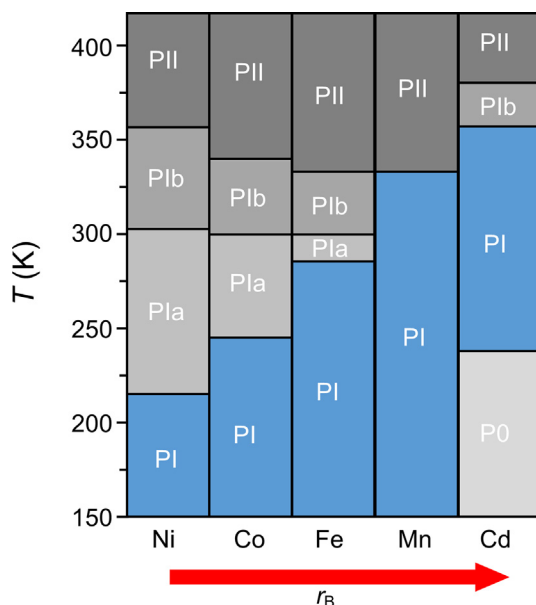
Fig. 17. Temperature phase diagram for the [Pr$_4$N][M(dca)$_3$] (M = Mn^{2+}, Fe^{2+}, Co^{2+}, Ni^{2+}, Cd^{2+}) perovskites highlighting the influence of the internal chemical pressure on the transition temperature from polymorph PI to the next higher temperature polymorph. Data extracted from references [81,84].

[Cd(dca)$_3$] perovskites is highly anisotropic. For example, in the case of the Mn-compound at ambient temperature, the *ab*-plane compresses by 54.4(15) × 10^{-3} GPa^{-1}, meanwhile the *c*-axis compresses by 8.0(12) × 10^{-3} GPa^{-1}. This extremely large compressibility is due to an increase in degree of the cooperative octahedral tilting as well as to an increase in the columnar shifts, which make these materials easily to deform. These structural flexibility towards stress-deformation results into very low bulk modulus for [Pr$_4$N][Mn(dca)$_3$] and [Pr$_4$N][Cd(dca)$_3$] with values of 8.1 and 6.2 GPa, respectively. Such values demonstrate a much larger compressibility than in the case of other HOIPs, such as formate-perovskites, where the bulk moduli are found to be of between 14.0 and 39.2 GPa [125,127].

Actually, this pressure-responsiveness allows dicyamide-perovskites to exhibit a larger barocaloric coefficient (pressure dependence of the transition temperature or dT_t/dp) than in the rest of the HOIPs, which will directly impact on their balorcaloric performance [161]. Fig. 16 shows an Ashby plot of transition temperature (T_t) *versus* barocaloric coefficient (dT_t/dp) for different families of HOIPs.

In addition, M. Mączka *et al.* demonstrated that [Pr$_4$N][Mn(dca)$_3$] and [Pr$_4$N][Cd(dca)$_3$] compounds also exhibit new pressure-induced structural transitions at much larger pressures. The [Pr$_4$N][Mn(dca)$_3$] perovskite displays three transitions occurring at 0.4, 3 and 5 GPa [125], while the [Pr$_4$N][Cd(dca)$_3$] compound shows only one transition between 0.3 and 0.4 GPa [127].

Furthermore, these studies have encouraged the exploration of barocaloric effects in other families of HOIPs [161–163], such as formate-perovskites [162] and azide-perovskites [163]. In this context, the [Et$_3$(CH$_2$CH$_2$X)P][Mn(dca)$_3$] (X = F$^-$, Cl$^-$) compounds exhibit the largest transition entropy changes (ΔS = [101–111] J K^{-1} kg^{-1}) of all the dicyanamide-perovskites near room temperature (T_t = [300–330] K), which anticipates a larger barocaloric effect than in the case of the [Pr$_4$N][M(dca)$_3$] (M = Mn^{2+}, Cd^{2+}). However, they also exhibit a larger thermal hysteresis (T_h – T_c) which could increase the pressure required for inducing such effects [164]. On the other hand, these larger thermal hystereses, in addition to the large enthalpy changes, can be advantageous for solar thermal energy storage applications, as demonstrated in other hybrid materials [165,166].

In a correspondence with the externally applied pressure, we also reported that the internal chemical pressure can shift the transition temperature of dicyanamide-perovskites, specifically, in [Pr$_4$N][M(dca)$_3$] (M = Mn^{2+}, Fe^{2+}, Co^{2+}, Ni^{2+}, Cd^{2+}) perovskites [81,84]. Chemical pressure is a well-established physical variable that can affect the properties of perovskites, as widely reported in the case of oxide-perovskites and recently found in their dicyanamide analogues [81,84]. This internal pressure arises when the tolerance factor differs from the ideal value, and increases with increasing B-cation size and a reduction in the tolerance factor. Accordingly, the low-volume polymorph is stablized over a wider temperature range. This is indeed the case for the polymorph PI (S.G. $P\overline{4}2_1c$) of the [Pr$_4$N][M(dca)$_3$] compounds, which is stabilized at higher temperatures when the chemical pressure increases from B = Ni^{2+} to B = Cd^{2+}(Fig. 17). As a result, this strategy can be used to modulate the temperature at which a given functional property appears.

4.4. Magnetic, dielectric and ferroic properties

4.4.1. Magnetic properties and antiferromagnetic coupling

The magnetism of dicyanamide coordination polymers (with different denticity, coordination modes and topologies) has been extensively explored since it was first reported [133], and the main results have been compiled in several books and review articles

Table 4
Magnetic response and selected magnetic parameters observed in dicyanamide-perovskites.

Perovskite	Magnetic response	T_N (K)	C (cm^3/mol)	θ (K)	μ_{eff} (μ_B)	g value	Ref
[Et$_3$(CH$_2$CH$_2$F)P][Mn(dca)$_3$]	AFM	2.4	4.298	−3.51	–	–	[76]
[Et$_3$(CH$_2$CH$_2$ClP][Mn(dca)$_3$]	AFM	2.4	4.378	−2.57	–	–	[76]
[Et$_3$BnN][Mn(dca)$_3$]	AFM	–	4.47	−3.74	5.99	–	[73]
[Bu$_3$BnN][Mn(dca)$_3$]	AFM	–	4.1	−2.17	5.69	–	[73]
[Bu$_3$BnN][Co(dca)$_3$]	AFM	–	3.27	−30.8	4.85	–	[73]
[Ph$_3$S][Mn(dca)$_3$]	AFM	2.5	–	−3.7	–	1.954	[74]
[Pr$_4$N][Mn(dca)$_3$]	AFM	2.1	–	−2.4	–	1.954	[79]
[Pr$_4$N][Ni(dca)$_3$]	–	–	–	−4.7	–	2.261	[79]
[Cp*$_2$Fe][Mn(dca)$_3$]	–	–	–	–	6.43	–	[78]
[Cp*$_2$Fe][Co(dca)$_3$]	–	–	4.16	−20.6	6.37	–	[78]
[Cp*$_2$Fe][Ni(dca)$_3$]	AFM	1.78	–	−1.25	3.77	–	[78]
[Cp*$_2$Fe][Cd(dca)$_3$]	–	–	0.74	−1.9	2.4	–	[78]
[Cp*$_2$Co][Mn(dca)$_3$]	–	–	4.35	−3.5	5.86	1.99	[78]
[Cp*$_2$Co][Co(dca)$_3$]	Weak FM	–	3.45	−30.1	–	–	[78]
[Cp*$_2$Co][Ni(dca)$_3$]	AFM	–	1.14	−0.19	3.12	–	[78]

Note: T_N = Néel temperature, C = Curie constant, θ = Weiss constant, μ_{eff} = magnetic moment, g = Landé g-factor

Fig. 18. Dielectric permittivity *versus* temperature at ambient pressure for the (a) $[Pr_4N][Mn(dca)_3]$ (b) $[Pr_4N][Co(dca)_3]$ dicyanamide perovskites, and at different pressures for the same (c) Mn- and (d) Co-compounds. Figures adapted with permission from references [80,81].

[134,167]. In this section, we exclusively select and present the magnetic response for dicyanamide-perovskites (see Table 4).

A large number of dicyanamide-perovskites display paramagnetic metal cations in the B-position (i.e. Mn^{2+}, Co^{2+}, Ni^{2+}, etc.). These paramagnetic cations are linked through $\mu_{1,5}$-dca bridges that can act as a superexchange pathway for magnetic interaction. However, the M-dca-M distance is very long (>8 Å) and give rise to poor magnetic coupling. Accordingly, long-range magnetic interactions of dicyanamide-perovskites along the $[M(dca)_3]^-$ frameworks result in canted antiferromagnetism (AFM) or weak ferromagnetism (WFM) at temperatures of T_N < 2.5 K. Table 4 shows reported magnetism parameters for dicyanamide-perovskite.

Interestingly, in the case of $[Cp^*_2Fe][M(dca)_3]$ and $[Cp^*_2Co][M(dca)_3]$, the A-cation provides a new paramagnetic metallic center that shortens the M−M distances and that, in principle, could provide a new pathway of magnetic interactions. Here, the distances between the B-cations of the framework and the A-cations of the pseudo-cuboctahedral cavities are slightly shorter than the B-B distances. However, those distances can range between 7 and 8 Å and, therefore, the magnetic coupling is still weak. Furthermore, it should be noted that those metallic centers located in the A- and B-positions are linked by secondary bonds, so the magnetic superexchange is even weaker than in the B-B case. In turn, up to date, A-B magnetic coupling has not been observed in dicyanamide-perovskites, although this superexchange coud be strengthen in future studies by different strategies, as discussed in section 5 below.

4.4.2. Dielectric properties and antiferroelectric order

Structural transitions generally incite changes in the dielectric permittivity of materials. For this reason, the dielectric response of most dicyanamide-perovskites with phase transitions has already been explored, confirming dielectric anomalies related to these transitions. The compounds investigated exhibit two different dielectric anomalies, namely, step-like and peak-like anomalies.

In 2015, the first dielectric studies on $[Pr_4N][Mn(dca)_3]$ found a dielectric step-like anomaly related to its structural phase transition occurring at 330 K (Fig. 18a) [80]. The change in the dielectric response and in the structure was found to be related to order–disorder processes (configurational disordering) of both the dca anions and $[Pr_4N]^+$ cations, and out-of-centre displacements of the $[Pr_4N]^+$ cations, which are two of the main distortions described in section 3.3. Accordingly, these distortions give rise to an antiferroelectric (AFE) order below $T_t \sim 330$ K. These results not only provided the first evidence of thermally-induced dielectric switching in dicyanamide-perovskites but, together with the previously reported AFM order [79] (Table 4), revealed this compound as the first example of a multiferroic type-I material within the dicyanamide-perovskites family [80]. In 2016, the same group reported dielectric studies on the analogue Fe-, Co- and Ni-compounds, which showed a peak-like anomaly at low-temperature and two step-like anomalies at higher temperatures (Fig. 18b) [81]. Moreover, since the dielectric anomalies are also related to phase transitions, they may be shifted in temperature
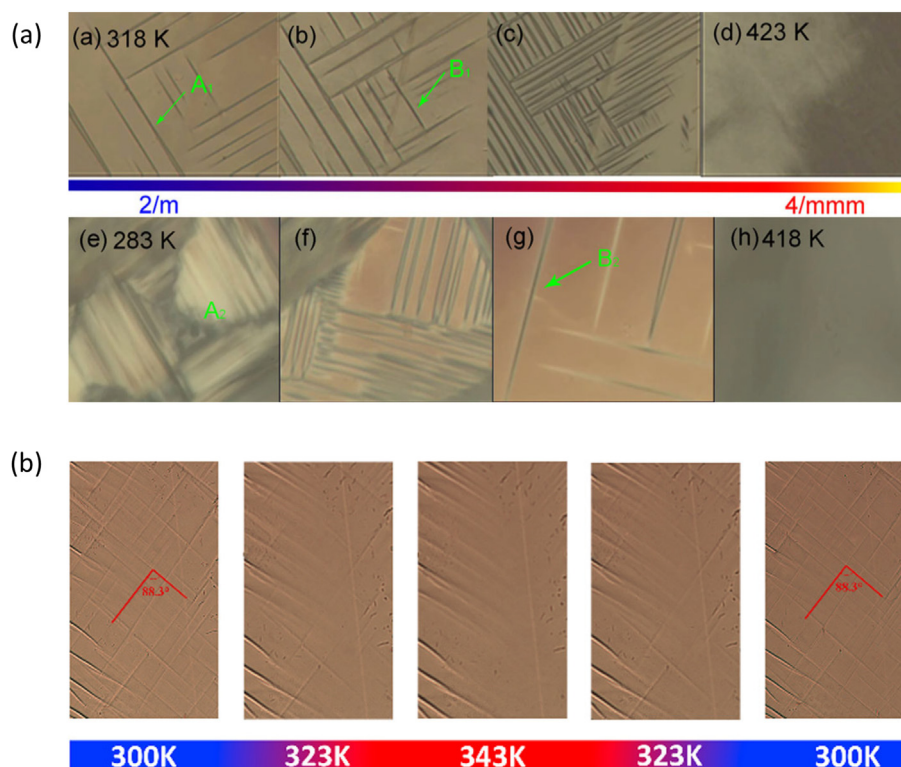
**Fig. 19.** (a) Evolution of the domain structures of the [Et$_3$(CH$_2$CH$_2$Cl)P][Mn(dca)$_3$] (top images) and [Et$_3$(CH$_2$CH$_2$F)P][Mn(dca)$_3$] (bottom images), and (b) [Pr$_3$(CH$_3$CHCH$_2$OH) N][Mn(dca)$_3$] perovskites, observed by polarized microscopy. Images reproduced with permission from references [76,77].

upon the application of external pressure, as previously explained for the structural transitions (Fig. 18**c-d**).

Later studies from M. Mączka et al. [127] showed that the analogous [Pr$_4$N][Cd(dca)$_3$] compound presents two step-like dielectric anomalies related to the reported structural transitions [84,127]. Interestingly, the activation energy of their dielectric studies (complemented with Raman and electron paramagnetic resonance analysis) revealed that such responses are strongly related to the [Pr$_4$N]$^+$ tumbling motions (that freeze at low temperature) and large distortions of the [Cd(dca)$_3$]$^-$ framework [127].

In addition, Fu et al. were able to tune the dielectric response (and associated structural transitions) of [Pr$_4$N][Mn(dca)$_3$]. They replaced one of the propyl groups of the [Pr$_4$N]$^+$ cation with either 2-hydroxy-propyl (CH$_2$CHOHCH$_3$) or 2-hydroxy-1-methyl-ethyl (CH$_3$CHCH$_2$OH) groups [77]. In the first case, they were able to reduce the transition temperature of the original phase transition from 330 K down to 207 K, while maintaining the step-like dielectric anomaly (Table 3). In the second compound they induced three completely new structural and dielectric step-like transitions (Table 3).

The dielectric behaviour of other families of dicyanamide-perovskites has also been explored. For example, in 2017, D.-W. Fu, Q. Ye et al. studied the response of dicyanamide-perovskites with alkylphosphonium (AP) cations in the A-site [76,82,83,85]. They observed that the [AP][Mn(dca)$_3$], (AP = [Et$_3$(n-Pr)P]$^+$, [Et$_3$(CH$_2$CHCH$_2$)P]$^+$, [Et$_3$(CH$_2$OCH$_3$)P]$^+$) perovskites display a single step-like dielectric anomaly related to a reversible phase transition [83], meanwhile the [Et$_3$(n-Pr)P][Cd(dca)$_3$] perovskite shows up to three step-like dielectric anomalies associated with the same number of reversible structural transitions [82]. Additionally, they reported the dielectric response of [Et$_3$(CH$_2$CH$_2$X)P][M(dca)$_3$] (M = Mn^{2+}, Cd^{2+}, X = F$^-$, Cl$^-$). They also found step-like dielectric anomalies related to multiple phase transitions. Their data also showed that the thermal hysteresis of the dielectric transitions
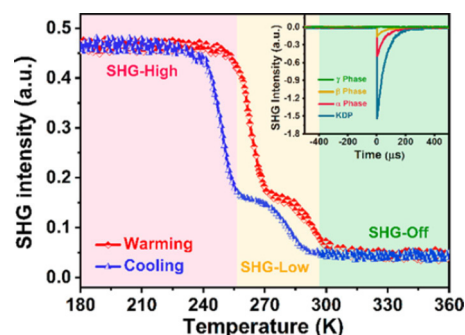
Fig. 20. Two-step switching of NLO of the [Pr$_3$(CH$_3$CHCH$_2$OH)N][Mn(dca)$_3$] perovskite, corresponding to two structural transitions. Insert: comparison of SHG signals of the different phases and KDP. The figure has been reproduced with permission from reference [77].

largely increases upon replacing Cl$^-$ with F$^-$ [85,76], which could be used to rationally design on–off dielectric switches working in different temperature windows.

4.4.3. Ferroelastic properties

The first studies on ferroelasticity in dicyanamide-perovskites were also performed by D.-W. Fu et al., [76,85] who discovered that the structural transitions found in the [Et$_3$(CH$_2$CH$_2$X)P][M(dca)$_3$] (M = Mn^{2+}, Cd^{2+}, X = F$^-$, Cl$^-$) compounds belonged to the 94 species of ferroelastic phase transitions described by Aizu notation [168].

In [Et$_3$(CH$_2$CH$_2$F)P][Mn(dca)$_3$], [Et$_3$(CH$_2$CH$_2$Cl)P][Mn(dca)$_3$] and [Et$_3$(CH$_2$CH$_2$F)P][Cd(dca)$_3$], the authors found two structural transitions from 2/m to mmm, and from mmm to 4/mmm, whose corresponding Aizu notation are mmmF2/m and 4/mmmFmmm respectively [168]. Meanwhile, [Et$_3$(CH$_2$CH$_2$F)P][Cd(dca)$_3$] did not exhibit ferroelastic transitions. In the observed ferroelastic transi-

Table 5
Selected optical parameters related to the absorption and photoluminescence of reported dicyanamide-perovskites.

Perovskite	λ_{abs} (nm)	d-d transitions	Optical E_g (eV)	λ_{exc} (nm)	λ_{emis} (nm)	τ (μs)	Ref.
$[Pr_4N][Mn(dca)_3]$	315	$^6A_1g(S) \rightarrow {}^4A_2g(F)$	5.17	420	626	5.88	[126]
	348	$^6A_1g(S) \rightarrow {}^4E(D)$					
	375	$^6A_1g(S) \rightarrow {}^4T_2g(D)$					
	414	$^6A_1g(S) \rightarrow {}^4A_1g, {}_4Eg(G)$					
	464	$^6A_1g(S) \rightarrow {}^4T_2g(G)$					
	575	$^6A_1g(S) \rightarrow {}^4T_1g(G)$					
$[Pr_4N][Cd(dca)_3]$	–	–	5.02	266	440, 510 (300 K)	4.64	[126]
$[Bu_3MeN][Mn(dca)_3]$	347	$^6A_1g(S) \rightarrow {}^4E(D)$	4.95	420	547, 652	–	[75]
	375	$^6A_1g(S) \rightarrow 4T_2g(D)$					
	414	$^6A_1g(S) \rightarrow {}^4A_1g, {}_4Eg(G)$					
	465	$^6A_1g(S) \rightarrow {}^4T_2g(G)$					
	573	$^6A_1g(S) \rightarrow {}^4T_1g(G)$					
$[Bu_3MeN][Fe(dca)_3]$	913	$^5T_2g(D) \rightarrow {}^5Eg(D)$	4.25			–	[75]
	1193	$^5T_2g(D) \rightarrow {}^5Eg(D)$					
$[Bu_3MeN][Co(dca)_3]$	481	$^4T_1(F) \rightarrow {}^4T_1(P)$	3.90			–	[75]
	513	$^4T_1(F) \rightarrow {}^2T_2(G)$					
	643	$^4T_1(F) \rightarrow {}^2E$					
	1152	$^4T_1(F) \rightarrow {}^2T_1(G)$					
$[Bu_3MeN][Ni(dca)_3]$	386	$^3A_2g(F) \rightarrow {}^3T_1g(P)$	4.35			–	[75]
	630	$^3A_2g(F) \rightarrow {}^3T_1g(F)$					
	1057	$^3A_2g(F) \rightarrow {}^3T_2g(F)$					
$[Et_3(n-Pr)P][Cd(dca)_3]$	–	–	–	325	525, 573	–	[82]

Note: λ_{abs} = maximum absorption wavelength, E_g = band gap, λ_{exc} = maximum excitation wavelength, λ_{emi} = maximum emission wavelength, τ = photoluminescence lifetime.

tions, the symmetry elements were doubled (from 2/m to mmm and from mmm to 4/mmm) and, which should result in two domain orientations. The authors confirmed the orientation change of the domains by using polarized microscopy while heating the sample (Fig. 19a) [76].

Further studies highlighted another ferroelastic transition in the $[Pr_3(CH_3CHCH_2OH)N][Mn(dca)_3]$ compound [77]. In this case, the authors identified a transition with Aizu notation 4/mmmFmmm. Moreover, they also used variable-temperature polarized microscopy to observe the domain evolution (Fig. 19b). In the low-temperature phase (at 300 K), they found a striped domain structure with flat domain walls forming angles of 90°, which suggested a symmetry decrease related to the disappearance of the 4-fold axis. Meanwhile, upon increasing the temperature to above the transition temperature, the domains disappeared [77].

4.5. Optical properties

Solid-state materials that can reversibly change from non–centrosymmetric to centrosymmetric structures can act as nonlinear optical (NLO) switches, which are optical transistors that can modulate the emitted output light with another light input. These NLO materials are of great interest in optical communication, photoelectric devices, and information processing. In that regard, $[Et_3(n-Pr)P][Mn(dca)_3]$ [83], $[Et_3(CH_2OCH_3)P][Mn(dca)_3]$ [83], $[Et_3(n-Pr)P][Cd(dca)_3]$ [82], $[Et_3(CH_2CH_2Cl)P][Cd(dca)_3]$ [85], $[Pr_4N][Mn(dca)_3]$ [126], $[Pr_4N][Cd(dca)_3]$ [126] and $[Pr_3(CH_3CHCH_2OH)N][Mn(dca)_3]$ [77] are active in second harmonic generation (SHG), and Q. Ye et al. [83] suggested that dicyanamide-perovskites could be used as NLO switches tuned by guest cations and triggered by temperature. Remarkably, the $[Pr_3(CH_3CHCH_2OH)N][Mn(dca)_3]$ perovskite was reported as the first molecular ferroelastic with two-step NLO switching (Fig. 20) [77].

Additionally, there are a few studies of dicyanamide-perovskites presenting absorption and photoluminiscence properties in the range of UV-Vis-NIR (Table 5), and is the case for $[Pr_4N][M(dca)_3]$ (M = Mn^{2+}, Cd^{2+}), $[Bu_3MeN][M(dca)_3]$ (M = Mn^{2+}, Fe^{2+}, Co^{2+}, Ni^{2+}) and $[Et_3(n-Pr)P][Cd(dca)_3]$. The diffuse reflectance spectra of the compounds investigated shows an intense absorption band below 300 nm (attributed to M−dca charge-transfer transitions) and some additional bands at larger wavelengths with lower

intensity (attributed to d-d electronic transitions of the different B-cations). The optical band gaps, E_g, of these compounds range from 3.90 to 5.17 eV (Table 5).

Moreover, the Mn-compounds under excitation of λ_{exc} = 420 nm exhibit broad emissions at λ_{emi} = [547–652] nm due to "forbidden" $^4T_{1g}(G) \rightarrow {}^6A_{1g}(S)$ d-d transition of the Mn^{2+} cations [75,126]. $[Bu_3MeN][Mn(dca)_3]$ exhibits a red-shift in emission upon decreasing temperature [75], while the emission peaks do not get displaced in the case of $[Pr_4N][Mn(dca)_3]$ [126]. Upon UV excitation (λ_{exc} = 266 nm), $[Pr_4N][Cd(dca)_3]$ [126] exhibits a broad bluish-white emission with two maxima located at 440 and 510 nm at room temperature. This compound shows a luminescence decay of τ = 4.64 μs, which slightly smaller than that of the Mn-analogue (τ = 5.88 μs). Even more interesting, the emission of this compound exhibits a blue shift upon increasing the temperature from 80 K to 250 K, while it shows a red shift when heating from 250 K to 375 K [126]. On the other hand, the $[Et_3(n-Pr)P][Cd(dca)_3]$ perovskite [82] shows a weak emission with two maxima at 525 and 573 nm under an excitation of λ_{exc} = 325 nm, which does not show any shift as a function of temperature. Meanwhile, as in the case of all studied compounds, the emission intensity increases at lower temperatures. This is due to slow motions at low temperature, which increases the framework rigidity and reduces the non-radiation energy losses [82].

It is worth noting that the presence of excitons in these compounds has not been yet discussed in the literature. Nevertheless, we would like to point out here that the observed absorption and emission spectra show characteristics compatible with their presence. Should this point be confirmed, dicyanamide-perovskites may have a future application as white-emission materials for LED lights.

5. Future perspectives

Since their discovery in 2003, dicyanamide-perovskites have arisen as a new class of materials with multifunctional properties and are of interest for different technological applications, including dielectric and/or magnetic switches, low-pressure solid-state barocaloric refrigerants, or precursors for oil-recovery nanomaterials. Even more recently, these materials have been used to obtain melt-quenched glasses that lie between organic and inorganic spe-

cies in their mechanical and thermal properties. The low thermal conductivities of $[Pr_4N][M(dca)_3]$ (M = Co^{2+}, Fe^{2+}, Mn^{2+}) glasses were found to be accompanied by moderate electrical conductivities, which may give rise to applications as thermoelectric glass materials [131]. The work also raises the possibility of liquid-based processing of the dca perovskites, given their observed low viscosities. Work on recrystallisation could allow for large-scale fabrication of grain-boundary free materials.

In this review, we have also demonstrated that this singular family of compounds exhibits characteristics on the borderline between dense HOIPs and porous MOFs. Indeed, in the last years, they have been shown to exhibit very high flexibilities and pressure responses, relatively low densities, low harnesses and elastic moduli, along with wide cavities that can allocate large cations, which resemble the features of MOFs. Moreover, and also similar to MOFs, they have been used as precursors of nanostructured carbon materials and glasses. However, and different from other porous hybrids, dicyanamide-perovskites have not yet shown any gas absorption capacity, and the principle of electrical neutrality prevents them from desorbing the guest molecules in the A-site cubooctahedral cavities without collapsing the structure.

In that regard, it should be noted that dicyanamide-perovskites were firstly explored around 15 years ago, which highlights the youth of this materials that have already shown very promising properties for different technological applications. In addition, these emerging studies can open new frontiers in the field that can attract the interest of chemists, physicists, materials scientists and engineers. For example, one of the striking features of dicyanamide-perovskites is the very large responsiveness towards pressure. Meanwhile, one of the challenges is still to find strong ferromagnetic and ferroelectric coupling within this family of compounds. In turn, it seems very plausible that the application of large pressures could easily induce new ferromagnetic and ferroelectric phases. Furthermore, by chemical modifications it could be possible to design paramagnetic A-cations that could strongly interact with paramagnetic B-cations through short A-B distances, enhancing magnetic superexchanges.

On the other hand, if we focus on the very large size of the pseudo-cuboctahedral cavities, we can anticipate that these materials could be used to capture and/or store low-volume molecules (i.e. hydrogen storage), whose release could potentially be controlled by external stimuli modification of the crystal structure. Moreover, by using trivalent transition metal cations (Al^{3+}, Fe^{3+}, Cr^{3+}, etc.) it would be possible to introduce neutrally charged A-molecules in the pseudo-cuboctaheral cavities, which could lead to adsorption/desorption processes, or molecular exchange, transport and delivery. Even more, the here observed $\pi\cdots\pi$ interactions can be engineered in order to design charge-transport, π-stacking ferroelectrics, and photoresponsive and optoelectronic materials. In addition, another yet unexplored field is the nanoestructuration of dicyanamide-perovskites. The control of the nanostructure in these materials could lead to an enhancement of their thermal properties, such as transition latent heat, thermal conductivity and/or thermal hysteresis, which would directly impact on their barocaloric performance and thermal energy storage capacity.

Regarding the crystal structure of this rich family of HOIPs, we have compiled many different and interesting structural distortions and we have provided a new method for calculating the tolerance factor of HOIPs. This compiled and rationalized information will help with the better understanding of structure-properties relationship in future studies and, ultimately, will lead towards a rational design of dicyanamide-perovskites for the desired applications. At this point, it should be noted that a deeper exploration of distortions and tilting engineering remains a challenge due to the very large number of degrees of freedom of these systems. Therefore, future studies must be focused on these aspects, which can

lead to a better control of the functional and multifunctional (i.e. ferroelectricity, multiferroicity) and thermal properties (i.e. barocaloric effects, thermal energy storage).

In summary, dicyanamide-perovskites are a very young and very promising sub-class of HOIPs with many interesting properties for technological applications. But what is more encouraging is the frontiers and challenges that the recent studies have opened around this innovative family of compounds.

Declaration of Competing Interest

The authors declare that they have no known competing financial interests or personal relationships that could have appeared to influence the work reported in this paper.

Acknowledgements

References

[1] G. Rose, Beschreibung einiger neuen Mineralien des Urals, Ann. Phys. 126 (8) (1840) 652–656, https://doi.org/10.1002/andp.18401260807.
[2] V.M. Goldschmidt, Die Gesetze der Krystallochemie, Naturwissenschaften 14 (21) (1926) 477–485, https://doi.org/10.1007/BF01507527.
[3] H.D. Megaw, Crystal structure of barium titanate, Nature 155 (1945) 484–485, https://doi.org/10.1038/155484b0.
[4] R.J.D. Tilley, Perovskites: structure-property relationships, Wiley, West Sussex, 2016.
[5] F.S. Galasso, Structure, Properties and Preparation of Perovskite-Type Compounds, Oxford (1969), https://doi.org/10.1016/B978-0-08-012744-6.50006-9.
[6] J.B. Goodenough, W. Gräper, F. Holtzberg, D.L. Huber, R.A. Lefever, J.M. Longo, T.R. McGuire, S. Methfessel, Magnetic and Other Properties of Oxides and Related Compounds, Springer, Berlin Heidelberg, 1970, https://doi.org/10.1007/b19968.
[7] W. Li, Z. Wang, F. Deschler, S. Gao, R.H. Friend, A.K. Cheetham, Chemically diverse and multifunctional hybrid organic-inorganic perovskites, Nat. Rev. Mater. 2 (16099) (2017), https://doi.org/10.1038/natrevmats.2016.99.
[8] L.G. Tejuca, J.L.G. Fierro, Properties and Applications Perovskite-type Oxides, Marcel Dekker, New York, 1993.
[9] A. von Hippel, Ferroelectricity, domain structure, and phase transitions of barium titanate, Rev. Mod. Phys. 22 (3) (1950) 221–237, https://doi.org/10.1103/RevModPhys.22.221.
[10] J.G. Bednorz, K.A. Muller, Possible high Tc superconductivity in the Ba-La-Cu-O system, Zeitschrift Für Phys. B Condens. Matter. 64 (1986) 189–193.
[11] M.K. Wu, J.R. Ashburn, C.J. Torng, P.H. Hor, R.L. Meng, L. Gao, Z.J. Huang, Y.Q. Wang, C.W. Chu, Superconductivity at 93 K in a new mixed-phase Y-Ba-Cu-O compound system at ambient pressure, Phys. Rev. Lett. 58 (1987) 908, https://doi.org/10.1103/PhysRevLett.58.908.
[12] G.H. Jonker, J.H. Van Santen, Ferromagnetic compounds of manganese with perovskite structure, Physica 16 (3) (1950) 337–349, https://doi.org/10.1016/0031-8914(50)90033-4.
[13] S. Jin, T.H. Tiefel, M. McCormack, R.A. Fastnacht, R. Ramesh, L.H. Chen, Thousandfold change in resistivity in magnetoresistive La-Ca-Mn-O films, Science. 264 (1994) 413–415. https://doi.org/10.1126/science.264.5157.413.
[14] S.-W. Cheong, M. Mostovoy, Multiferroics: a magnetic twist for ferroelectricity, Nat. Mater. 6 (1) (2007) 13–20, https://doi.org/10.1038/nmat1804.
[15] M.M. Lee, J. Teuscher, T. Miyasaka, T.N. Murakami, H.J. Snaith, Efficient hybrid solar cells based on meso-superstructured organometal halide perovskites, Science 338 (6107) (2012) 643–647, https://doi.org/10.1126/science.1228604.

[16] J. Burschka, N. Pellet, S.-J. Moon, R. Humphry-Baker, P. Gao, M.K. Nazeeruddin, M. Grätzel, Sequential deposition as a route to high-performance perovskite-sensitized solar cells, Nature 499 (2013) 316, https://doi.org/10.1038/nature12340.

[17] C.A. Bremner, M. Simpson, W.T.A. Harrison, New molecular perovskites: Cubic C4N2H12·NH4 Cl3·H2O and 2-H hexagonal C6N2H14·NH4Cl3, J. Am. Chem. Soc. 124 (2002) 10960–10961, https://doi.org/10.1021/ja027484e.

[18] H.Y. Ye, Y.Y. Tang, P.F. Li, W.Q. Liao, J.X. Gao, X.N. Hua, H. Cai, P.P. Shi, Y.M. You, R.G. Xiong, Metal-free three-dimensional perovskite ferroelectrics, Science 361 (2018) 151–155, https://doi.org/10.1126/science.aas9330.

[19] G.-M. Fan, C. Shi, L. Qiao, H.-J. Li, H.-Y. Ye, Photoluminescence of Sn2+-I−-mixed molecular perovskites, J. Mater. Chem. C 6 (31) (2018) 8349–8352, https://doi.org/10.1039/C8TC02587H.

[20] K. Li, L.-Y. Dong, H.-X. Xu, Y. Qin, Z.-G. Li, M. Azeem, W. Li, X.-H. Bu, Electronic structures and elastic properties of a family of metal-free perovskites, Mater. Chem. Front. 3 (8) (2019) 1678–1685, https://doi.org/10.1039/C9QM00133F.

[21] H. Remy, G. Laves, Über Chlorokomplexsalze des zweiwertigen Kupfers., Berichte Der Dtsch, Chem. Gesellschaft A B Ser. 66 (3) (1933) 401–407, https://doi.org/10.1002/cber.19330660319.

[22] W. Dieter, CH3NH3PbX3, ein Pb(II)-system mit kubischer perowskitstruktur, Zeitschrift Für Naturforsch. B 33 (1978) 1443–1445, https://doi.org/10.1515/znb-1978-1214.

[23] E. Sletten, L.H. Jensen, The crystal structure of dimethylammonium copper(II) formate, NH2(CH2)2[Cu(OOCH)3], Acta Crystallogr, Sect. B Struct. Crystallogr. Cryst. Chem. 29 (1973) 1752–1756, https://doi.org/10.1107/s0567740873005480.

[24] B. Zhou, Y. Imai, A. Kobayashi, Z.-M. Wang, H. Kobayashi, Giant Dielectric Anomaly of a Metal-Organic Perovskite with Four-Membered Ring Ammonium Cations, Angew Chemie 123 (48) (2011) 11643–11647, https://doi.org/10.1002/ange.201105111.

[25] Z. Duan, Z. Wang, S. Gao, Irreversible transformation of chiral to achiral polymorph of K[Co(HCOO)3]: Synthesis, structures, and magnetic properties, Dalt. Trans. 40 (2011) 4465–4473, https://doi.org/10.1039/c0dt01701a.

[26] J.C. Tan, P. Jain, A.K. Cheetham, Influence of ligand field stabilization energy on the elastic properties of multiferroic MOFs with the perovskite architecture, Dalt. Trans. 41 (2012) 3949–3952, https://doi.org/10.1039/c2dt12300b.

[27] R. Shang, X. Sun, Z.-M. Wang, S. Gao, Zinc-diluted magnetic metal formate perovskites: Synthesis, structures, and magnetism of [CH3NH3][MnxZn1−x (HCOO) 3] (x=0-1), Chem. - An Asian J. 7 (7) (2012) 1697–1707, https://doi.org/10.1002/asia.201200139.

[28] A. Rossin, M.R. Chierotti, G. Giambastiani, R. Gobetto, M. Peruzzini, Amine-templated polymeric Mg formates: Crystalline scaffolds exhibiting extensive hydrogen bonding, CrystEngComm 14 (2012) 4454–4460, https://doi.org/10.1039/c2ce25048a.

[29] B. Pato-Doldán, L.C. Gómez-Aguirre, J.M. Bermúdez-García, M. Sánchez-Andújar, A. Fondado, J. Mira, S. Castro-García, M.A. Señarís-Rodríguez, Coexistence of magnetic and electrical order in the new perovskite-like (C3N2H5)[Mn(HCOO)3] formate, RSC Adv. 3 (44) (2013) 22404, https://doi.org/10.1039/c3ra43165g.

[30] E. Eikeland, N. Lock, M. Filsø, M. Stingaciu, Y. Shen, J. Overgaard, B.B. Iversen, Alkali metal ion templated transition metal formate framework materials: Synthesis, crystal structures, ion migration, and magnetism, Inorg. Chem. 53 (19) (2014) 10178–10188, https://doi.org/10.1021/ic501152j.

[31] K.-L. Hu, M. Kurmoo, Z. Wang, S. Gao, Metal-organic perovskites: Synthesis, structures, and magnetic properties of [C(NH2)3][MII(HCOO)3] (M=Mn, Fe Co, Ni, Cu, and Zn; C(NH2)3=guanidinium), Chem. - A Eur. J. 15 (44) (2009) 12050–12064, https://doi.org/10.1002/chem.200901605.

[32] Z. Wang, B. Zhang, T. Otsuka, K. Inoue, H. Kobayashi, M. Kurmoo, Anionic NaCl-type frameworks of [MnII (HCOO)3 −], templated by alkylammonium, exhibit weak ferromagnetism, Dalt. Trans. (15) (2004) 2209–2216, https://doi.org/10.1039/B404466E.

[33] D.-W. Fu, W. Zhang, H.-L. Cai, Y.i. Zhang, J.-Z. Ge, R.-G. Xiong, S.D. Huang, T. Nakamura, A multiferroic perdeutero metal-organic framework, Angew. Chemie - Int. Ed. 50 (50) (2011) 11947–11951, https://doi.org/10.1002/anie.201103265.

[34] R.E. Marsh, On the structure of Zn(C4H8N2O6), Acta Crystallogr, Sect. C Cryst. Struct. Commun. 42 (1986) 1327–1328, https://doi.org/10.1107/s0108270186092399.

[35] B.-Q. Wang, H.-B. Yan, Z.-Q. Huang, Z. Zhang, Reversible high-temperature phase transition of a manganese(II) formate framework with imidazolium cations, Acta Crystallogr, Sect. C Cryst. Struct. Commun. 69 (6) (2013) 616–619, https://doi.org/10.1107/S0108270113012638.

[36] S.a. Chen, R. Shang, K.-L. Hu, Z.-M. Wang, S. Gao, [NH2NH3][M(HCOO)3] (M = Mn2+, Zn2+, Co2+ and Mg2+): structural phase transitions, prominent dielectric anomalies, and negative thermal expansion, and magnetic ordering, Inorg. Chem. Front. 1 (1) (2014) 83–98, https://doi.org/10.1039/C3QI00034F.

[37] M. Mączka, A. Ciupa, A. Gagor, A. Sieradzki, A. Pikul, B. Macalik, M. Drozd, Perovskite metal formate framework of [NH2-CH +-NH2]Mn(HCOO)3]: Phase transition, magnetic, dielectric, and phonon properties, Inorg. Chem. 53 (10) (2014) 5260–5268, https://doi.org/10.1021/ic500479e.

[38] J.Q. Liu, J. Wu, J. Wang, L. Lu, C. Daiguebonne, G. Calvez, O. Guillou, H. Sakiyama, N.S. Weng, M. Zeller, Temperature identification on two 3D Mn(ii) metal-organic frameworks: Syntheses, adsorption and magnetism, RSC Adv. 4 (2014) 20605–20611, https://doi.org/10.1039/c4ra02609h.

[39] M. Mączka, A. Gągor, M. Ptak, W. Paraguassu, T.A. da Silva, A. Sieradzki, A. Pikul, Phase Transitions and Coexistence of Magnetic and Electric Orders in the Methylhydrazinium Metal Formate Frameworks, Chem. Mater. 29 (5) (2017) 2264–2275, https://doi.org/10.1021/acs.chemmater.6b05249.

[40] R. Shang, S.a. Chen, Z.-M. Wang, S. Gao, A Copper-Formate Framework Showing a Simple to Helical Antiferroelectric Transition with Prominent Dielectric Anomalies and Anisotropic Thermal Expansion, and Antiferromagnetism, Chem. - A Eur. J. 20 (48) (2014) 15872–15883, https://doi.org/10.1002/chem.201403466.

[41] R. Shang, G.-C. Xu, Z.-M. Wang, S. Gao, Phase transitions, prominent dielectric anomalies, and negative thermal expansion in three high thermally stable ammonium magnesium-formate frameworks, Chemistry 20 (4) (2014) 1146–1158, https://doi.org/10.1002/chem.201303425.

[42] L.C. Gómez-Aguirre, B. Pato-Doldán, A. Stroppa, S. Yáñez-Vilar, L. Bayarjargal, B. Winkler, S. Castro-García, J. Mira, M. Sánchez-Andújar, M.A. Señarís-Rodríguez, Room-temperature polar order in [NH4][Cd(HCOO)3] - A hybrid inorganic-organic compound with a unique perovskite architecture, Inorg. Chem. 54 (5) (2015) 2109–2116, https://doi.org/10.1021/ic502218n.

[43] A. Ciupa, M. Mączka, A. Gągor, A. Pikul, E. Kucharska, J. Hanuza, A. Sieradzki, Synthesis, crystal structure, magnetic and vibrational properties of formamidine-templated Co and Fe formates, Polyhedron 85 (2015) 137–143, https://doi.org/10.1016/j.poly.2014.08.008.

[44] B. Pato-Doldán, L.C. Gómez-Aguirre, A.P. Hansen, J. Mira, S. Castro-García, M. Sánchez-Andújar, M.A. Señarís-Rodríguez, V.S. Zapf, J. Singleton, Magnetic transitions and isotropic: Versus anisotropic magnetic behaviour of [CH3NH3][M(HCOO)3] M = Mn2+, Co2+, Ni2+, Cu2+ metal-organic perovskites, J. Mater. Chem. C 4 (47) (2016) 11164–11172, https://doi.org/10.1039/C6TC03992H.

[45] M. Boča, I. Svoboda, F. Renz, H. Fuess, Poly[methylammonium tris(μ2-formato-κ2O: O′′)cobalt(II)], Acta Crystallogr, Sect. C Cryst. Struct. Commun. 60 (12) (2004) m631–m633, https://doi.org/10.1107/S0108270104025776.

[46] I.E. Collings, J.A. Hill, A.B. Cairns, R.I. Cooper, A.L. Thompson, J.E. Parker, C.C. Tang, A.L. Goodwin, Compositional dependence of anomalous thermal expansion in perovskite-like ABX3 formates, Dalt. Trans. 45 (10) (2016) 4169–4178, https://doi.org/10.1039/C5DT03263F.

[47] M. Mączka, N.L. Marinho Costa, A. Gągor, W. Paraguassu, A. Sieradzki, J. Hanuza, Structural, thermal, dielectric and phonon properties of perovskite-like imidazolium magnesium formate, Phys. Chem. Chem. Phys. 18 (20) (2016) 13993–14000, https://doi.org/10.1039/C6CP01353H.

[48] J.M. Bermúdez-García, A. García-Fernández, A. Andrada-Chacón, J. Sánchez-Benítez, W. Ren, S. Hu, T. Gu, H. Xiang, M. Biczysko, S. Castro-García, M. Sánchez-Andújar, A. Stroppa, M.A. Señarís-Rodríguez, Pressure-induced reversible framework rearrangement and increased polarization in the polar [NH4][Cd(HCOO)3] hybrid perovskite, Inorg. Chem. Front. 6 (9) (2019) 2379–2386, https://doi.org/10.1039/C9QI00749K.

[49] X.-Y. Wang, L. Gan, S.-W. Zhang, S. Gao, Perovskite-like metal formates with weak ferromagnetism and as precursors to amorphous materials, Inorg. Chem. 43 (15) (2004) 4615–4625, https://doi.org/10.1021/ic0498081.

[50] A. Rossin, A. Ienco, F. Costantino, T. Montini, B. Di Credico, M. Caporali, L. Gonsalvi, P. Fornasiero, M. Peruzzini, Phase transitions and CO2 adsorption properties of polymeric magnesium formate, Cryst. Growth Des. 8 (9) (2008) 3302–3308, https://doi.org/10.1021/cg800181q.

[51] P. Jain, N.S. Dalal, B.H. Toby, H.W. Kroto, A.K. Cheetham, Order-disorder antiferroelectric phase transition in a hybrid inorganic-organic framework with the perovskite architecture, J. Am. Chem. Soc. 130 (2008) 10450–10451. http://www.ncbi.nlm.nih.gov/pubmed/18636729.

[52] P. Jain, V. Ramachandran, R.J. Clark, H.D. Zhou, B.H. Toby, N.S. Dalal, H.W. Kroto, A.K. Cheetham, Multiferroic behavior associated with an order-disorder hydrogen bonding transition in metal-organic frameworks (MOFs) with the perovskite ABX3 architecture, J. Am. Chem. Soc. 131 (2009) 13625–13627. http://www.ncbi.nlm.nih.gov/pubmed/19725496.

[53] M. Sánchez-Andújar, S. Presedo, S. Yáñez-Vilar, S. Castro-García, J. Shamir, M.A. Señarís-Rodríguez, Characterization of the order-disorder dielectric transition in the hybrid organic-inorganic perovskite-like formate Mn (HCOO)3[(CH3)2NH2], Inorg. Chem. 49 (4) (2010) 1510–1516, https://doi.org/10.1021/ic901872g.

[54] S. Gao, S.W. Ng, Poly[dimethylammonium [tris(μ2-formato-κ2O: O′)cadmate (II)]], Acta Crystallogr. Sect. E Struct. Rep. Online. 66 (2010) 3–7. https://doi.org/10.1107/S1600536810046830.

[55] S. Peschel, D. Babel, Zur Kristallstruktur der Cyanoelpasolithe [N(CH3)4] 2CsCo(CN)6 und [H3NCH3]2NaFe(CN)6, Zeitschrift Fur Naturforsch. - Sect. B J. Chem. Sci. 49 (1994) 1373–1380, https://doi.org/10.1515/znb-1994-1011.

[56] W. Zhang, Y. Cai, R.-G. Xiong, H. Yoshikawa, K. Awaga, Exceptional dielectric phase transitions in a perovskite-type cage compound, Angew. Chemie - Int. Ed. 49 (37) (2010) 6608–6610, https://doi.org/10.1002/anie.201001208.

[57] W. Zhang, H.-Y. Ye, R. Graf, H.W. Spiess, Y.-F. Yao, R.-Q. Zhu, R.-G. Xiong, Tunable and switchable dielectric constant in an amphidynamic crystal, J. Am. Chem. Soc. 135 (14) (2013) 5230–5233, https://doi.org/10.1021/ja3110335.

[58] X.i. Zhang, X.-D. Shao, S.-C. Li, Y. Cai, Y.-F. Yao, R.-G. Xiong, W. Zhang, Dynamics of a caged imidazolium cation-toward understanding the order-disorder phase transition and the switchable dielectric constant, Chem. Commun. 51 (22) (2015) 4568–4571, https://doi.org/10.1039/C4CC08693G.

[59] W.-J. Xu, K.-P. Xie, Z.-F. Xiao, W.-X. Zhang, X.-M. Chen, Controlling Two-Step Phase Transitions and Dielectric Responses by A-Site Cations in Two

Perovskite-like Coordination Polymers, Cryst. Growth Des. 16 (12) (2016) 7212–7217, https://doi.org/10.1021/acs.cgd.6b01404.

[60] W.-J. Xu, S.-L. Chen, Z.-T. Hu, R.-B. Lin, Y.-J. Su, W.-X. Zhang, X.-M. Chen, The cation-dependent structural phase transition and dielectric response in a family of cyano-bridged perovskite-like coordination polymers, Dalt. Trans. 45 (10) (2016) 4224–4229, https://doi.org/10.1039/C5DT03481G.

[61] K. Qian, F. Shao, Z. Yan, J. Pang, X. Chen, C. Yang, A perovskite-type cage compound as a temperature-triggered dielectric switchable material, CrystEngComm 18 (40) (2016) 7671–7674, https://doi.org/10.1039/C6CE01421F.

[62] C. Shi, C.-H. Yu, W. Zhang, Predicting and Screening Dielectric Transitions in a Series of Hybrid Organic-Inorganic Double Perovskites via an Extended Tolerance Factor Approach, Angew. Chemie - Int. Ed. 55 (19) (2016) 5798–5802, https://doi.org/10.1002/anie.201602028.

[63] W.-J. Xu, P.-F. Li, Y.-Y. Tang, W.-X. Zhang, R.-G. Xiong, X.-M. Chen, A Molecular Perovskite with Switchable Coordination Bonds for High-Temperature Multiaxial Ferroelectrics, J. Am. Chem. Soc. 139 (18) (2017) 6369–6375, https://doi.org/10.1021/jacs.7b01334.

[64] M. Trzebiatowska, A. Gągor, L. Macalik, P. Peksa, A. Sieradzki, Phase transition in the extreme: A cubic-to-triclinic symmetry change in dielectrically switchable cyanide perovskites, Dalt. Trans. 48 (42) (2019) 15830–15840, https://doi.org/10.1039/C9DT03250A.

[65] F.A. Mautner, H. Krischner, C. Kratky, Tetramethylammonium-calcium-triazid, Darstellung und Kristallstruktur, Monatshefte Ffir Chemie 119 (1988) 1245–1249, https://doi.org/10.1007/BF00624743.

[66] F.A. Mautner, S. Hanna, R. Cortés, L. Lezama, M.G. Barandika, T. Rojo, Crystal structure and spectroscopic and magnetic properties of the manganese(II) and copper(II) azido-tetramethylammonium systems, Inorg. Chem. 38 (21) (1999) 4647–4652, https://doi.org/10.1021/ic981373s.

[67] X.-H. Zhao, X.-C. Huang, S.-L. Zhang, D. Shao, H.-Y. Wei, X.-Y. Wang, Cation-dependent magnetic ordering and room-temperature bistability in azido-bridged perovskite-type compounds, J. Am. Chem. Soc. 135 (43) (2013) 16006–16009, https://doi.org/10.1021/ja407654n.

[68] Z.Y. Du, Y.P. Zhao, W.X. Zhang, H.L. Zhou, C.T. He, W. Xue, B.Y. Wang, X.M. Chen, Above-room-temperature ferroelastic phase transition in a perovskite-like compound [N(CH3)4][Cd(N3)3], Chem. Commun. 50 (2014) 1989–1991, https://doi.org/10.1039/c3cc48581a.

[69] Z.-Y. Du, Y.-Z. Sun, S.-L. Chen, B.o. Huang, Y.-J. Su, T.-T. Xu, W.-X. Zhang, X.-M. Chen, Insight into the molecular dynamics of guest cations confined in deformable azido coordination frameworks, Chem. Commun. 51 (86) (2015) 15641–15644, https://doi.org/10.1039/C5CC06863K.

[70] Z.-Y. Du, T.-T. Xu, B.o. Huang, Y.-J. Su, W. Xue, C.-T. He, W.-X. Zhang, X.-M. Chen, Switchable guest molecular dynamics in a perovskite-like coordination polymer toward sensitive thermoresponsive dielectric materials, Angew. Chemie - Int. Ed. 54 (3) (2015) 914–918, https://doi.org/10.1002/anie.201408491.

[71] K. Qian, Y. Xu, Z. Wang, J. Yang, Synthesis, crystal structure, and magnetic properties of an azido-bridged Mn(II) complex [C3H5NH3][Mn(N3)3], Zeitschrift Fur Naturforsch. - Sect. B J. Chem. Sci. 72 (2017) 409–413, https://doi.org/10.1515/znb-2016-0267.

[72] J. Yang, Y. Huang, T. Fang, K. Qian, X.F. Yu, Y.C. Ai, J.L. Ye, X.Y. Li, Synthesis, crystal structure, and magnetic properties of a multicage compound: [(Me)2EtNH][Mn(N3)3] with a perovskite-related structure, Zeitschrift Fur Naturforsch. - Sect. B J. Chem. Sci. 74 (2019) 335–339, https://doi.org/10.1515/znb-2018-0183.

[73] M.L. Tong, J. Ru, Y.M. Wu, X.M. Chen, H.C. Chang, K. Mochizuki, S. Kitagawa, Cation-templated construction of three-dimensional α-Po cubic-type [M(dca) 3]- networks: Syntheses, structures and magnetic properties of A[M(dca)3] (dca = dicyanamide; for A = benzyltributylammonium, M = Mn2+, Co2+; for A = benzyltriethylammonium, M = Mn2, New J. Chem. 27 (2003) 779–782, https://doi.org/10.1039/b300760j.

[74] J.A. Schlueter, J.L. Manson, K.A. Hyzer, U. Geiser, Spin canting in the 3D anionic dicyanamide structure (SPh 3)Mn(dca)3 (Ph = phenyl, dca = dicyanamide), Inorg. Chem. 43 (14) (2004) 4100–4102, https://doi.org/10.1021/ic035398p.

[75] M. Mączka, A. Gągor, M. Ptak, D. Stefańska, L. Macalik, A. Pikul, A. Sieradzki, Structural, phonon, magnetic and optical properties of novel perovskite-like frameworks of TriBuMe[M(dca)3] (TriBuMe = tributylmethylammonium; Dca = dicyanamide; M = Mn2+, Fe2+, Co2+, Ni2+), Dalt. Trans. 48 (34) (2019) 13006–13016, https://doi.org/10.1039/C9DT02924A.

[76] M.-M. Zhao, L. Zhou, P.-P. Shi, X. Zheng, X.-G. Chen, J.-X. Gao, L. He, Q. Ye, C.-M. Liu, D.-W. Fu, 3D Organic-lnorganic Perovskite Ferroelastic Materials with Two Ferroelastic Phases: [Et 3 P(CH 2) 2 F][Mn(dca) 3] and [Et 3 P(CH 2) 2 Cl][Mn(dca) 3], Chem. - A Eur. J. 25 (25) (2019) 6447–6454, https://doi.org/10.1002/chem.v25.2510.1002/chem.201900771.

[77] Z.-B. Liu, L. He, P.-P. Shi, Q. Ye, D.-W. Fu, A Three-Dimensional Molecular Perovskite Ferroelastic with Two-Step Switching of Quadratic Nonlinear Optical Properties Tuned by Molecular Chiral Design, J. Phys. Chem. Lett. 11 (19) (2020) 7960–7965, https://doi.org/10.1021/acs.jpclett.0c02235.

[78] P.M. Van der Werff, E. Martínez-Ferrero, S.R. Batten, P. Jensen, C. Ruiz-Pérez, M. Almeida, J.C. Waerenborgh, J.D. Cashion, B. Moubaraki, J.R. Galán-Mascarós, J.M. Martínez-Agudo, E. Coronado, K.S. Murray, Hybrid materials containing organometallic cations and 3-D anionic metal dicyanamide networks of type [Cp*2M][M'(dca)3], Dalt. Trans. (2) (2005) 285–290, https://doi.org/10.1039/B415275A.

[79] J.A. Schlueter, J.L. Manson, U. Geiser, Structural and magnetic diversity in tetraalkylammonium salts of anionic M[N(CN) 2] 3 (M = Mn and Ni) three-dimensional coordination polymers, Inorg. Chem. 44 (9) (2005) 3194–3202, https://doi.org/10.1021/ic0484598.

[80] J.M. Bermúdez-García, M. Sánchez-Andújar, S. Yáñez-Vilar, S. Castro-García, R. Artiaga, J. López-Beceiro, L. Botana, Á. Alegría, M.A. Señarís-Rodríguez, Role of Temperature and Pressure on the Multisensitive Multiferroic Dicyanamide Framework [TPrA][Mn(dca)3] with Perovskite-like Structure, Inorg. Chem. 54 (24) (2015) 11680–11687, https://doi.org/10.1021/acs.inorgchem.5b01652.

[81] J.M. Bermúdez-García, M. Sánchez-Andújar, S. Yáñez-Vilar, S. Castro-García, R. Artiaga, J. López-Beceiro, L. Botana, A. Alegría, M.A. Señarís-Rodríguez, Multiple phase and dielectric transitions on a novel multi-sensitive [TPrA][M (dca)3] (M: Fe2+, Co2+ and Ni2+) hybrid inorganic-organic perovskite family, J. Mater. Chem. C 4 (22) (2016) 4889–4898, https://doi.org/10.1039/C6TC00723F.

[82] L. Zhou, X. Zheng, P.-P. Shi, Z. Zafar, H.-Y. Ye, D.-W. Fu, Q. Ye, Switchable Nonlinear Optical and Tunable Luminescent Properties Triggered by Multiple Phase Transitions in a Perovskite-Like Compound, Inorg. Chem. 56 (6) (2017) 3238–3244, https://doi.org/10.1021/acs.inorgchem.6b02508.

[83] F.-J. Geng, L. Zhou, P.-P. Shi, X.-L. Wang, X. Zheng, Y.i. Zhang, D.-W. Fu, Q. Ye, Perovskite-type organic-inorganic hybrid NLO switches tuned by guest cations, J. Mater. Chem. C 5 (6) (2017) 1529–1536, https://doi.org/10.1039/C6TC05105G.

[84] J.M. Bermúdez-García, S. Yáñez-Vilar, A. García-Fernández, M. Sánchez-Andújar, S. Castro-García, J. López-Beceiro, R. Artiaga, M. Dilshad, X. Moya, M.A. Señarís-Rodríguez, Giant barocaloric tunability in [(CH3CH2CH2)4N]Cd [N(CN)2]3 hybrid perovskite, J. Mater. Chem. C 6 (37) (2018) 9867–9874, https://doi.org/10.1039/C7TC03136J.

[85] M.-M. Zhao, L. Zhou, P.-P. Shi, X. Zheng, X.-G. Chen, J.-X. Gao, F.-J. Geng, Q. Ye, D.-W. Fu, Halogen substitution effects on optical and electrical properties in 3D molecular perovskites, Chem. Commun. 54 (94) (2018) 13275–13278, https://doi.org/10.1039/C8CC07052K.

[86] G. Thiele, D. Messer, S-Thiocyanato- und N-Isothiocyanato-Bindungsisomerie in den Kristallstrukturen von RbCd(SCN)3 und CsCd(SCN)3, ZAAC - J. Inorg. Gen. Chem. 464 (1) (1980) 255–267, https://doi.org/10.1002/zaac.19804640124.

[87] K.-P. Xie, W.-J. Xu, C.-T. He, B.o. Huang, Z.-Y. Du, Y.-J. Su, W.-X. Zhang, X.-M. Chen, Order-disorder phase transition in the first thiocyanate-bridged double perovskite-type coordination polymer: [NH4]2[NiCd(SCN)6], CrystEngComm 18 (24) (2016) 4495–4498, https://doi.org/10.1039/C6CE00898D.

[88] Y.-L. Sun, X.-B. Han, W. Zhang, Structural Phase Transitions and Dielectric Switching in a Series of Organic-Inorganic Hybrid Perovskites ABX3 (X=ClO4− or BF4−), Chem. - A Eur. J. 23 (46) (2017) 11126–11132, https://doi.org/10.1002/chem.201702228.

[89] Y.-L. Sun, C. Shi, W. Zhang, Distinct room-temperature dielectric transition in a perchlorate-based organic-inorganic hybrid perovskite, Dalt. Trans. 46 (48) (2017) 16774–16778, https://doi.org/10.1039/C7DT03798H.

[90] Y.-L. Sun, X.-B. Han, W. Zhang, Molecular perovskite high-energetic materials, Sci. China Mater. 61 (2018) 1123, https://doi.org/10.1007/s40843-017-9219-9.

[91] S.-L. Chen, Y.u. Shang, C.-T. He, L.-Y. Sun, Z.-M. Ye, W.-X. Zhang, X.-M. Chen, Optimizing the oxygen balance by changing the A-site cations in molecular perovskite high-energetic materials, CrystEngComm 20 (46) (2018) 7458–7463, https://doi.org/10.1039/C8CE01350K.

[92] Y. Wu, T. Binford, J.A. Hill, S. Shaker, J. Wang, A.K. Cheetham, Hypophosphite hybrid perovskites: A platform for unconventional tilts and shifts, Chem. Commun. 54 (30) (2018) 3751–3754, https://doi.org/10.1039/C8CC00907D.

[93] Y. Wu, S. Shaker, F. Brivio, R. Murugavel, P.D. Bristowe, A.K. Cheetham, Mn (H2POO)3: A New Family of Hybrid Perovskites Based on the Hypophosphite Ligand, J. Am. Chem. Soc. 139 (47) (2017) 16999–17002, https://doi.org/10.1021/jacs.7b09417.

[94] P. Schouwink, M.B. Ley, A. Tissot, H. Hagemann, T.R. Jensen, Ľ. Smrčok, R. Černý, Structure and properties of complex hydride perovskite materials, Nat. Commun. 5 (1) (2014), https://doi.org/10.1038/ncomms6706.

[95] J. Lefebvre, D. Chartrand, D.B. Leznoff, Synthesis, structure and magnetic properties of 2-D and 3-D [cation]{M[Au(CN)2]3} (M = Ni, Co) coordination polymers, Polyhedron 26 (9-11) (2007) 2189–2199, https://doi.org/10.1016/j.poly.2006.10.045.

[96] J.A. Hill, A.L. Thompson, A.L. Goodwin, Dicyanometallates as Model Extended Frameworks, J. Am. Chem. Soc. 138 (18) (2016) 5886–5896, https://doi.org/10.1021/jacs.5b13446.

[97] C.N.R. Rao, A.K. Cheetham, A. Thirumurugan, Hybrid inorganic-organic materials: A new family in condensed matter physics, J. Phys. Condens. Matter. 20 (8) (2008) 083202, https://doi.org/10.1088/0953-8984/20/8/083202.

[98] B. Saparov, D.B. Mitzi, Organic-Inorganic Perovskites: Structural Versatility for Functional Materials Design, Chem. Rev. 116 (7) (2016) 4558–4596, https://doi.org/10.1021/acs.chemrev.5b00715.

[99] A. Walsh, Principles of chemical bonding and band gap engineering in hybrid organic-inorganic halide perovskites, J. Phys. Chem. C 119 (11) (2015) 5755–5760, https://doi.org/10.1021/jp512420b.

[100] A. Salzer, Nomenclature of organometallic compounds of the transition elements, Pure Appl. Chem. 71 (1999) 1557–1585, https://doi.org/10.1351/pac199971101557.

[101] S.R. Batten, N.R. Champness, X.M. Chen, J. Garcia-Martinez, S. Kitagawa, L. Öhrström, M. O'Keeffe, M.P. Suh, J. Reedijk, Coordination polymers, metal-

organic frameworks and the need for terminology guidelines, CrystEngComm 14 (2012) 3001–3004, https://doi.org/10.1039/c2ce06488j.

[102] M. Cude, IUPAC Provisional Recommendations on metal-organic framework and coordination polymer terminology, CrystEngComm Blog (2013).

[103] H. Li, M. Eddaoudi, M. Yaghi, M. O'Keeffe, O.M. Yaghi, Design and synthesis of an exceptionally stable and highly porous metal-organic framework, Nature 402 (1999) 276–279, https://doi.org/10.1038/46248.

[104] A.K. Cheetham, C.N.R. Rao, There's room in the middle, Science 318 (5847) (2007) 58–59, https://doi.org/10.1126/science.1147231.

[105] G. Férey, Hybrid porous solids: past, present, future, Chem. Soc. Rev. 37 (1) (2008) 191–214, https://doi.org/10.1039/B618320B.

[106] H.-C. Zhou, J.R. Long, O.M. Yaghi, Introduction to metal-organic frameworks, Chem. Rev. 112 (2) (2012) 673–674, https://doi.org/10.1021/cr300014x.

[107] H. Furukawa, N. Ko, Y.B. Go, N. Aratani, S.B. Choi, E. Choi, A.Ö. Yazaydin, R.Q. Snurr, M. O'Keeffe, J. Kim, O.M. Yaghi, Ultrahigh porosity in metal-organic frameworks, Science 329 (2010) 424–428, https://doi.org/10.1126/science.1192160.

[108] M. Ding, R.W. Flaig, H.-L. Jiang, O.M. Yaghi, Carbon capture and conversion using metal-organic frameworks and MOF-based materials, Chem. Soc. Rev. 48 (10) (2019) 2783–2828, https://doi.org/10.1039/C8CS00829A.

[109] M.T. Kapelewski, T. Runčevski, J.D. Tarver, H.Z.H. Jiang, K.E. Hurst, P.A. Parilla, A. Ayala, T. Gennett, S.A. FitzGerald, C.M. Brown, J.R. Long, Record High Hydrogen Storage Capacity in the Metal-Organic Framework Ni2(m-dobdc) at Near-Ambient Temperatures, Chem. Mater. 30 (22) (2018) 8179–8189, https://doi.org/10.1021/acs.chemmater.8b03276.

[110] J.A. Mason, M. Veenstra, J.R. Long, Evaluating metal-organic frameworks for natural gas storage, Chem. Sci. 5 (1) (2014) 32–51, https://doi.org/10.1039/C3SC52633J.

[111] N. Hanikel, M.S. Prévot, F. Fathieh, E.A. Kapustin, H. Lyu, H. Wang, N.J. Diercks, T.G. Glover, O.M. Yaghi, Rapid Cycling and Exceptional Yield in a Metal-Organic Framework Water Harvester, ACS Cent. Sci. 5 (10) (2019) 1699–1706, https://doi.org/10.1021/acscentsci.9b00745.

[112] W. Xu, O.M. Yaghi, Metal-Organic Frameworks for Water Harvesting from Air, Anywhere, Anytime, ACS Cent. Sci. 6 (8) (2020) 1348–1354, https://doi.org/10.1021/acscentsci.0c00678.

[113] S. Wang, J.S. Lee, M. Wahiduzzaman, J. Park, M. Muschi, C. Martineau-Corcos, A. Tissot, K.H. Cho, J. Marrot, W. Shepard, G. Maurin, J.-S. Chang, C. Serre, A robust large-pore zirconium carboxylate metal–organic framework for energy-efficient water-sorption-driven refrigeration, Nat. Energy 3 (11) (2018) 985–993, https://doi.org/10.1038/s41560-018-0261-6.

[114] S.K. Henninger, H.A. Habib, C. Janiak, MOFs as adsorbents for low temperature heating and cooling applications, J. Am. Chem. Soc. 131 (8) (2009) 2776–2777, https://doi.org/10.1021/ja808444z.

[115] M.-X. Wu, Y.-W. Yang, Metal-Organic Framework (MOF)-Based Drug/Cargo Delivery and Cancer Therapy, Adv. Mater. 29 (23) (2017) 1606134, https://doi.org/10.1002/adma.201606134.

[116] C. Orellana-Tavra, E.F. Baxter, T. Tian, T.D. Bennett, N.K.H. Slater, A.K. Cheetham, D. Fairen-Jimenez, Amorphous metal-organic frameworks for drug delivery, Chem. Commun. 51 (73) (2015) 13878–13881, https://doi.org/10.1039/C5CC05237H.

[117] T.D. Bennett, A.K. Cheetham, Amorphous metal-organic frameworks, Acc. Chem. Res. 47 (5) (2014) 1555–1562, https://doi.org/10.1021/ar5000314.

[118] R. Gaillac, P. Pullumbi, K.A. Beyer, K.W. Chapman, D.A. Keen, T.D. Bennett, F.-X. Coudert, Liquid metal–organic frameworks, Nat. Mater. 16 (11) (2017) 1149–1154, https://doi.org/10.1038/nmat4998.

[119] H.L.B. Boström, M.S. Senn, A.L. Goodwin, Recipes for improper ferroelectricity in molecular perovskites, Nat. Commun. 9 (2018) 1–7, https://doi.org/10.1038/s41467-018-04764-x.

[120] L.C. Gómez-Aguirre, B. Pato-Doldán, A. Stroppa, L.-M. Yang, T. Frauenheim, J. Mira, S. Yáñez-Vilar, R. Artiaga, S. Castro-García, M. Sánchez-Andújar, M.A. Señarís-Rodríguez, Coexistence of Three Ferroic Orders in the Multiferroic Compound [(CH3)4N][Mn(N3)3] with Perovskite-Like Structure, Chem. - A Eur. J. 22 (23) (2016) 7863–7870, https://doi.org/10.1002/chem.201503445.

[121] L.C. Gómez-Aguirre, B. Pato-Doldán, J. Mira, S. Castro-García, M.A. Señarís-Rodríguez, M. Sánchez-Andújar, J. Singleton, V.S. Zapf, Magnetic Ordering-Induced Multiferroic Behavior in [CH3NH3][Co(HCOO)3] Metal–Organic Framework, J. Am. Chem. Soc. 138 4 (2016) 1122–1125, https://doi.org/10.1021/jacs.5b11688.

[122] W.-J. Xu, Z.-Y. Du, W.-X. Zhang, X.-M. Chen, Structural phase transitions in perovskite compounds based on diatomic or multiatomic bridges, CrystEngComm 18 (41) (2016) 7915–7928, https://doi.org/10.1039/C6CE01485B.

[123] T.M. Brenner, D.A. Egger, L. Kronik, G. Hodes, D. Cahen, Hybrid organic - Inorganic perovskites: Low-cost semiconductors with intriguing charge-transport properties, Nat. Rev. Mater. 1 (2016) 1–16, https://doi.org/10.1038/natrevmats.2015.7.

[124] L.J. Ji, S.J. Sun, Y. Qin, K. Li, W. Li, Mechanical properties of hybrid organic-inorganic perovskites, Coord. Chem. Rev. 391 (2019) 15–29, https://doi.org/10.1016/j.ccr.2019.03.020.

[125] M. Mączka, I.E. Collings, F.F. Leite, W. Paraguassu, Raman and single-crystal X-ray diffraction evidence of pressure-induced phase transitions in a perovskite-like framework of [(C3H7)4N] [Mn(N(CN)2)3], Dalt. Trans. 48 (25) (2019) 9072–9078, https://doi.org/10.1039/C9DT01648A.

[126] M. Mączka, D. Stefańska, J.K. Zaręba, M. Nyk, A. Sieradzki, Temperature-dependent luminescence and second-harmonic generation of perovskite-type manganese and cadmium dicyanamide frameworks templated by

tetrapropylammonium cations, J. Alloys Compd. 821 (2020) 153464, https://doi.org/10.1016/j.jallcom.2019.153464.

[127] M. Mączka, M. Ptak, A. Gągor, A. Sieradzki, P. Peksa, G. Usevicius, M. Simenas, F.F. Leite, W. Paraguassu, Temperature- and pressure-dependent studies of a highly flexible and compressible perovskite-like cadmium dicyanamide framework templated with protonated tetrapropylamine, J. Mater. Chem. C 7 (8) (2019) 2408–2420, https://doi.org/10.1039/C8TC06401F.

[128] J.A. Schlueter, U. Geiser, J.L. Manson, Anionic dicyanamide frameworks as possible components of multifunctional materials, J. Phys. IV Fr. 114 (2004) 475–479, https://doi.org/10.1051/jp4:2004114111.

[129] A. Ciupa-Litwa, M. Ptak, J. Hanuza, E. Kucharska, K. Beć, Comparative studies of vibrational properties and phase transitions in perovskite-like frameworks of [(C3H7)4N][M(N(CN)2)3] with M=Mn, Co, Ni, J. Raman Spectrosc. 50 (2019) 1561–1571, https://doi.org/10.1002/jrs.5627.

[130] J.M. Bermúdez-García, M. Sánchez-Andújar, S. Castro-García, J. López-Beceiro, R. Artiaga, M.A. Señarís-Rodríguez, Giant barocaloric effect in the ferroic organic-inorganic hybrid [TPrA][Mn(dca)3] perovskite under easily accessible pressures, Nat. Commun. 8 (15715) (2017), https://doi.org/10.1038/ncomms15715.

[131] B.K. Shaw, A.R. Hughes, M. Ducamp, S. Moss, A. Debnath, A.F. Sapnik, M.F. Thorne, L.N. McHugh, A. Pugliese, D.S. Keeble, P. Chater, J.M. Bermudez-Garcia, X. Moya, S.K. Saha, D.A. Keen, F.-X. Coudert, F. Blanc, T.D. Bennett, Melting of hybrid organic–inorganic perovskites, Nat. Chem. 13 (2021) 778–785, https://doi.org/10.1038/s41557-021-00681-7.

[132] J.M. Bermúdez-García, S. Yáñez-Vilar, A. García-Fernández, M. Sánchez-Andújar, S. Castro-García, J. Mira, J.A. Moreira, T.A. Centeno, M.A. Señarís-Rodríguez, A simple in situ synthesis of magnetic M@CNTs by thermolysis of the hybrid perovskite [TPrA][M(dca)3], New J. Chem. 41 (8) (2017) 3124–3133, https://doi.org/10.1039/C6NJ03672D.

[133] A.M. Golub, H. Köhler, V.V. Skopenko, Chemistry of Pseudohalides, Elsevier, Oxford, 1986.

[134] S.R. Batten, S.M. Neville, D.R. Turner, Coordination Polymers: Design, Royal Society of Chemistry, Cambridge, Analysis and Application, 2008.

[135] N.G. Connelly, T. Damhus, R.M. Hartshorn, A.T. Hutton, NOMENCLATURE OF INORGANIC CHEMISTRY IUPAC Recommendations 2005 IUPAC Periodic Table of the Elements Fn No, 2005. https://doi.org/10.1039/ja069710g.

[136] J. Gao, K. Ye, M. He, W.W. Xiong, W. Cao, Z.Y. Lee, Y. Wang, T. Wu, F. Huo, X. Liu, Q. Zhang, Tuning metal-carboxylate coordination in crystalline metal-organic frameworks through surfactant media, J. Solid State Chem. 206 (2013) 27–31, https://doi.org/10.1016/j.jssc.2013.07.031.

[137] M.J. Turner, J.J. McKinnon, S.K. Wolff, D.J. Grimwood, P.R. Spackman, D. Jayatilaka, M.A. Spackman, CrystalExplorer17, (2017).

[138] A.S. Mitchell, M.A. Spackman, Molecular Surfaces from the Promolecule: A Comparison with Hartree-Fock Ab Initio Electron Density Surfaces, J. Comput. Chem. 21 (2000) 933–942, https://doi.org/10.1002/1096-987X(200008)21:11<933::AID-JCC3>3.0.CO;2-F.

[139] A.M. Glazer, The classification of tilted octahedra in perovskites, Acta Crystallogr. Sect. B Struct. Crystallogr. Cryst. Chem. 28 (1972) 3384–3392, https://doi.org/10.1107/s0567740872007976.

[140] G. Kieslich, S. Sun, A.K. Cheetham, Solid-state principles applied to organic–inorganic perovskites: new tricks for an old dog, Chem. Sci. 5 (12) (2014) 4712–4715, https://doi.org/10.1039/C4SC02211D.

[141] G. Kieslich, S. Sun, A.K. Cheetham, An Extended Tolerance Factor Approach for Organic-Inorganic Perovskites, Chem. Sci. 6 (6) (2015) 3430–3433, https://doi.org/10.1039/C5SC00961H.

[142] S. Gholipour, A.M. Ali, J.-P. Correa-Baena, S.-H. Turren-Cruz, F. Tajabadi, W. Tress, N. Taghavinia, M. Grätzel, A. Abate, F. De Angelis, C.A. Gaggioli, E. Mosconi, A. Hagfeldt, M. Saliba, Globularity-Selected Large Molecules for a New Generation of Multication Perovskites, Adv. Mater. 29 (38) (2017) 1702005, https://doi.org/10.1002/adma.201702005.

[143] H.L.B. Boström, Tilts and shifts in molecular perovskites, CrystEngComm 22 (5) (2020) 961–968, https://doi.org/10.1039/C9CE01950B.

[144] H.L.B. Boström, A.L. Goodwin, Hybrid Perovskites, Metal–Organic Frameworks, and Beyond: Unconventional Degrees of Freedom in Molecular Frameworks, Acc. Chem. Res. 54 (5) (2021) 1288–1297, https://doi.org/10.1021/acs.accounts.0c00797.

[145] H.L.B. Boström, J.A. Hill, A.L. Goodwin, Columnar shifts as symmetry-breaking degrees of freedom in molecular perovskites, Phys. Chem. Chem. Phys. 18 (46) (2016) 31881–31894, https://doi.org/10.1039/C6CP05730F.

[146] Z.-Y. Du, Y.-P. Zhao, C.-T. He, B.-Y. Wang, W. Xue, H.-L. Zhou, J. Bai, B. Huang, W.-X. Zhang, X.-M. Chen, Structural Transition in the Perovskite-like Bimetallic Azido Coordination Polymers: (NMe4)2[B′·B″(N3)6](B′ =Cr3+, Fe3+; B″ =Na+, K+), Cryst. Growth Des. 14 (2014) 3903–3909, https://doi.org/10.1021/S1600536813022411.

[147] N.C. Burtch, J. Heinen, T.D. Bennett, D. Dubbeldam, M.D. Allendorf, Mechanical Properties in Metal-Organic Frameworks: Emerging Opportunities and Challenges for Device Functionality and Technological Applications, Adv. Mater. 30 (37) (2018) 1704124, https://doi.org/10.1002/adma.201704124.

[148] J.C. Tan, A.K. Cheetham, Mechanical properties of hybrid inorganic–organic framework materials: Establishing fundamental structure–property relationships, Chem. Soc. Rev. 40 (2011) 1059–1080, https://doi.org/10.1039/c0cs00163e.

[149] S. Horike, S. Shimomura, S. Kitagawa, Soft porous crystals, Nat. Chem. 1 (9) (2009) 695–704, https://doi.org/10.1038/nchem.444.

[150] A.J. Howarth, Y. Liu, P. Li, Z. Li, T.C. Wang, J.T. Hupp, O.K. Farha, Chemical, thermal and mechanical stabilities of metal-organic frameworks, Nat. Rev. Mater. 1 (2016) 1–15, https://doi.org/10.1038/natrevmats.2015.18.

[151] C. Healy, K.M. Patil, B.H. Wilson, L. Hermanspahn, N.C. Harvey-Reid, B.I. Howard, C. Kleinjan, J. Kolien, F. Payet, S.G. Telfer, P.E. Kruger, T.D. Bennett, The thermal stability of metal-organic frameworks, Coord. Chem. Rev. 419 (2020) 213388, https://doi.org/10.1016/j.ccr.2020.213388.

[152] J. Ma, A.P. Kalenak, A.G. Wong-Foy, A.J. Matzger, Rapid Guest Exchange and Ultra-Low Surface Tension Solvents Optimize Metal-Organic Framework Activation, Angew. Chemie - Int. Ed. 56 (46) (2017) 14618–14621, https://doi.org/10.1002/anie.v56.4610.1002/anie.201709187.

[153] A.M. Bumstead, M.F. Thorne, T.D. Bennett, Identifying the liquid and glassy states of coordination polymers and metal–organic frameworks, Faraday Discuss. 225 (2021) 210–225, https://doi.org/10.1039/D0FD00011F.

[154] A.M. Bumstead, M.L. Ríos Gómez, M.F. Thorne, A.F. Sapnik, L. Longley, J.M. Tuffnell, D.S. Keeble, D.A. Keen, T.D. Bennett, Investigating the melting behaviour of polymorphic zeolitic imidazolate frameworks, CrystEngComm 22 (21) (2020) 3627–3637, https://doi.org/10.1039/D0CE00408A.

[155] T.D. Bennett, Y. Yue, P. Li, A. Qiao, H. Tao, N.G. Greaves, T. Richards, G.I. Lampronti, S.A.T. Redfern, F. Blanc, O.K. Farha, J.T. Hupp, A.K. Cheetham, D.A. Keen, Melt-Quenched Glasses of Metal-Organic Frameworks, J. Am. Chem. Soc. 138 (10) (2016) 3484–3492, https://doi.org/10.1021/jacs.5b1322010.1021/jacs.5b13220.s001.

[156] P.G. Debenedetti, F.H. Stillinger, Supercooled liquids and the glass transition, Nature 410 (2001) 259, https://doi.org/10.1038/35065704.

[157] G.N. Greaves, Hybrid Glasses: From Metal Organic Frameworks and Co-ordination Polymers to Hybrid Organic Inorganic Perovskites, in: J.D. Musgraves, J. Hu, L. Calvez (Eds.), Springer Handb. Glas., Springer International Publishing, Cham, 2019: pp. 719–770. https://doi.org/10.1007/978-3-319-93728-1_21.

[158] X. Moya, S. Kar-Narayan, N.D. Mathur, Caloric materials near ferroic phase transitions, Nat. Mater. 13 (5) (2014) 439–450, https://doi.org/10.1038/nmat3951.

[159] P. Lloveras, A. Aznar, M. Barrio, P. Negrier, C. Popescu, A. Planes, L. Mañosa, E. Stern-Taulats, A. Avramenko, N.D. Mathur, X. Moya, J.L. Tamarit, Colossal barocaloric effects near room temperature in plastic crystals of neopentylglycol, Nat. Commun. 10 (1803) (2019), https://doi.org/10.1038/s41467-019-09730-9.

[160] B. Li, Y. Kawakita, S. Ohira-Kawamura, T. Sugahara, H. Wang, J. Wang, Y. Chen, S.I. Kawaguchi, S. Kawaguchi, K. Ohara, K. Li, D. Yu, R. Mole, T. Hattori, T. Kikuchi, S.–I. Yano, Z. Zhang, Z. Zhang, W. Ren, S. Lin, O. Sakata, K. Nakajima, Z. Zhang, Colossal barocaloric effects in plastic crystals, Nature 567 (7749) (2019) 506–510, https://doi.org/10.1038/s41586-019-1042-5.

[161] J.M. Bermúdez-García, M. Sánchez-Andújar, M.A. Señarís-Rodríguez, A New Playground for Organic-Inorganic Hybrids: Barocaloric Materials for Pressure-Induced Solid-State Cooling, J. Phys. Chem. Lett. 8 (18) (2017) 4419–4423, https://doi.org/10.1021/acs.jpclett.7b01845.

[162] M. Szafrański, W.-J. Wei, Z.-M. Wang, W. Li, A. Katrusiak, Research Update: Tricritical point and large caloric effect in a hybrid organic-inorganic perovskite, APL Mater. 6 (10) (2018) 100701, https://doi.org/10.1063/1.5049116.

[163] J. Salgado-Beceiro, A. Nonato, R.X. Silva, A. García-Fernández, M. Sánchez-Andújar, S. Castro-García, E. Stern-Taulats, M.A. Señarís-Rodríguez, X. Moya, J. M. Bermúdez-García, Near-room-temperature reversible giant barocaloric effects in [(CH3)4 N]Mn[N3]3 hybrid perovskite, Mater. Adv. 1 (9) (2020) 3167–3170, https://doi.org/10.1039/D0MA00652A.

[164] T. Hess, L.M. Maier, N. Bachmann, P. Corhan, O. Schäfer-Welsen, J. Wöllenstein, K. Bartholomé, Thermal hysteresis and its impact on the efficiency of first-order caloric materials, J. Appl. Phys. 127 (7) (2020) 075103, https://doi.org/10.1063/1.5132897.

[165] D. Li, X.-M. Zhao, H.-X. Zhao, L.-S. Long, L.-S. Zheng, Coexistence of Magnetic-Optic-Electric Triple Switching and Thermal Energy Storage in a Multifunctional Plastic Crystal of Trimethylchloromethyl Ammonium Tetrachloroferrate(III), Inorg. Chem. 58 (1) (2019) 655–662, https://doi.org/10.1021/acs.inorgchem.8b0283510.1021/acs.inorgchem.8b02835.s001.

[166] J. Salgado-Beceiro, J.M. Bermúdez-García, A.L. Llamas-Saiz, S. Castro-García, M.A. Señarís-Rodríguez, F. Rivadulla, M. Sánchez-Andújar, Multifunctional properties and multi-energy storage in the [(CH3)3 S][FeCl4] plastic crystal, J. Mater. Chem. C 8 (39) (2020) 13686–13694, https://doi.org/10.1039/D0TC04044D.

[167] S.R. Batten, K.S. Murray, Structure and magnetism of coordination polymers containing dicyanamide and tricyanomethanide, Coord. Chem. Rev. 246 (1–2) (2003) 103–130, https://doi.org/10.1016/S0010-8545(03)00119-X.

[168] K. Aizu, Possible species of ferromagnetic, ferroelectric, and ferroelastic crystals, Phys. Rev. B. 2 (3) (1970) 754–772, https://doi.org/10.1103/PhysRevB.2.754.

[169] L. Chen, W.Q. Liao, Y. Ai, J. Li, S. Deng, Y. Hou, Y.Y. Tang, Precise Molecular Design Toward Organic-Inorganic Zinc Chloride ABX3 Ferroelectrics, J. Am. Chem. Soc. 142 (2020) 6236–6243, https://doi.org/10.1021/jacs.0c00315.

[170] W.T.A. Harrison, Structural diversity in non-layered hybrid perovskites of the RMCl3 family, Angew. Chemie - Int. Ed. 49 (2010) 7684–7687, https://doi.org/10.1002/anie.201003541.

[171] J.D. Tornero, F.H. Cano, J. Payos, M. Martinez-Ripoll, X-ray single crystal analysis of the phase transitions in NH4MnCl3. Some Mossbauer-X-ray spectra relations, Ferroelectrics 19 (1) (1978) 123–130, https://doi.org/10.1080/00150197808237840.

[172] Y. Dang, C. Zhong, G. Zhang, D. Ju, L. Wang, S. Xia, H. Xia, X. Tao, Crystallographic investigations into properties of acentric hybrid perovskite single crystals NH(CH3)3SnX3 (X = Cl, Br), Chem. Mater. 28 (2016) 6968–6974, https://doi.org/10.1021/acs.chemmater.6b02653.

[173] S. Govinda, B.P. Kore, D. Swain, A. Hossain, C. De, T.N. Guru Row, D.D. Sarma, Critical Comparison of FAPbX3 and MAPbX3 (X = Br and Cl): How Do They Differ?, J Phys. Chem. C. 122 (2018) 13758–13766, https://doi.org/10.1021/acs.jpcc.8b00602.

[174] X.G. Chen, J.X. Gao, X.N. Hua, W.Q. Liao, Three-dimensional organic–inorganic hybrid sodium halide perovskite: C4H12N2·NaI3 and a hydrogen-bonded supramolecular three-dimensional network in 3C4H12N2·Nai4·3I·H2O, Acta Crystallogr. Sect. C Struct. Chem. 74 (2018) 728–733, https://doi.org/10.1107/S2053229618006885.

[175] C.C. Stoumpos, L. Frazer, D.J. Clark, Y.S. Kim, S.H. Rhim, A.J. Freeman, J.B. Ketterson, J.I. Jang, M.G. Kanatzidis, Hybrid germanium iodide perovskite semiconductors: Active lone pairs, structural distortions, direct and indirect energy gaps, and strong nonlinear optical properties, J. Am. Chem. Soc. 137 (2015) 6804–6819, https://doi.org/10.1021/jacs.5b01025.

[176] S. Ferrandin, A.M.Z. Slawin, W.T.A. Harrison, Syntheses and crystal structures of a new family of hybrid perovskites: C5H14N2Abr30.5H2O (A = K, rb, Cs), Acta Crystallogr. Sect. E Crystallogr. Commun. 75 (2019) 1243–1248, https://doi.org/10.1107/S2056989019010338.

[177] Q. Pan, Z.B. Liu, Y.Y. Tang, P.F. Li, R.W. Ma, R.Y. Wei, Y. Zhang, Y.M. You, H.Y. Ye, R.G. Xiong, A Three-Dimensional Molecular Perovskite Ferroelectric: (3-Ammoniopyrrolidinium)RbBr3, J. Am. Chem. Soc. 139 (2017) 3954–3957, https://doi.org/10.1021/jacs.7b00492.

[178] A. Jaffe, Y. Lin, C.M. Beavers, J. Voss, W.L. Mao, H.I. Karunadasa, High-pressure single-crystal structures of 3D lead-halide hybrid perovskites and pressure effects on their electronic and optical properties, ACS Cent. Sci. 2 (2016) 201–209, https://doi.org/10.1021/acscentsci.6b00055.

[179] I. Swainson, L. Chi, J.H. Her, L. Cranswick, P. Stephens, B. Winkler, D.J. Wilson, V. Milman, Orientational ordering, tilting and lone-pair activity in the perovskite methylammonium tin bromide, CH3NH3SnBr3, Acta Crystallogr. Sect. B Struct. Sci. 66 (2010) 422–429, https://doi.org/10.1107/S0108768110014734.

[180] Y. Takahashi, R. Obara, Z.Z. Lin, Y. Takahashi, T. Naito, T. Inabe, S. Ishibashi, K. Terakura, Charge-transport in tin-iodide perovskite CH3NH3SnI3: Origin of high conductivity, Dalt. Trans. 40 (2011) 5563–5568, https://doi.org/10.1039/c0dt01601b.

[181] C.C. Stoumpos, C.D. Malliakas, M.G. Kanatzidis, Semiconducting tin and lead iodide perovskites with organic cations: Phase transitions, high mobilities, and near-infrared photoluminescent properties, Inorg. Chem. 52 (2013) 9019–9038, https://doi.org/10.1021/ic401215x.

[182] Y. Shang, R.K. Huang, S.L. Chen,, C.T. He, Z.H. Yu, Z.M. Ye, W.X. Zhang, X.M. Chen, Metal-Free Molecular Perovskite High-Energetic Materials, Cryst. Growth Des. 20 (2020) 1891–1897, https://doi.org/10.1021/acs.cgd.9b01592.

[183] Inorganic Crystal Structure Database -, ICSD (2019).

[184] T. Loiseau, C. Serre, C. Huguenard, G. Fink, F. Taulelle, M. Henry, T. Bataille, G. Férey, A Rationale for the Large Breathing of the Porous Aluminum Terephthalate (MIL-53) Upon Hydration, Chem. - A Eur. J. 10 (2004) 1373–1382, https://doi.org/10.1002/chem.200305413.

[185] C. Serre, F. Millange, C. Thouvenot, M. Noguès, G. Marsolier, D. Louër, G. Férey, Very large breathing effect in the first nanoporous chromium(III)-based solids: MIL-53 or CrIII(OH)·{O2C-C6H4- CO2}·{HO2C-C6H4 -CO2H}x·H2Oy, J. Am. Chem. Soc. 124 (2002) 13519–13526, https://doi.org/10.1021/ja0276974.

[186] S.M. Hyun, J.H. Lee, G.Y. Jung, Y.K. Kim, T.K. Kim, S. Jeoung, S.K. Kwak, D. Moon, H.R. Moon, Exploration of Gate-Opening and Breathing Phenomena in a Tailored Flexible Metal-Organic Framework, Inorg. Chem. 55 (2016) 1920–1925, https://doi.org/10.1021/acs.inorgchem.5b02874.

[187] B.W. Hu, J.P. Zhao, E.C. Sañudo, F.C. Liu, Y.F. Zeng, X.H. Bu, Nickel(ii)–azido ferromagnetic chains in a 3D porous metal–organic framework with breathing guest molecules, Dalt. Trans. 1 (2008) 5556–5559, https://doi.org/10.1039/b812402g.

[188] P.K. Thallapally, J. Tian, M.R. Kishan, C.A. Fernandez, S.J. Dalgarno, P.B. McGrail, J.E. Warren, J.L. Atwood, Flexible (breathing) interpenetrated metal-organic frameworks for CO2 separation applications, J. Am. Chem. Soc. 130 (2008) 16842–16843, https://doi.org/10.1021/ja806391k.

[189] J. Xiao, Y. Wu, M. Li, B.Y. Liu, X.C. Huang, D. Li, Crystalline structural intermediates of a breathing metal-organic framework that functions as a luminescent sensor and gas reservoir, Chem. - A Eur. J. 19 (2013) 1891–1895, https://doi.org/10.1002/chem.201203515.

[190] S. Mukherjee, B. Joarder, A.V. Desai, B. Manna, R. Krishna, S.K. Ghosh, Exploiting framework flexibility of a metal-organic framework for selective adsorption of styrene over ethylbenzene, Inorg. Chem. 54 (2015) 4403–4408, https://doi.org/10.1021/acs.inorgchem.5b00206.

[191] P.V. Dau, M. Kim, S.J. Garibay, F.H.L. Münch, C.E. Moore, S.M. Cohen, Single-atom ligand changes affect breathing in an extended metal-organic framework, Inorg. Chem. 51 (2012) 5671–5676, https://doi.org/10.1021/ic202683s.

[192] L. Le Gong, X.F. Feng, F. Luo, Novel azo-Metal-Organic Framework Showing a 10-Connected bct Net, Breathing Behavior, and Unique Photoswitching Behavior toward CO2, Inorg. Chem. 54 (2015) 11587–11589, https://doi.org/10.1021/acs.inorgchem.5b02037.

[193] J. Heinen, A.D. Ready, T.D. Bennett, D. Dubbeldam, R.W. Friddle, N.C. Burtch, Elucidating the Variable-Temperature Mechanical Properties of a Negative

Thermal Expansion Metal-Organic Framework, ACS Appl. Mater. Interfaces 10 (2018) 21079–21083, https://doi.org/10.1021/acsami.8b06604.

[194] C.L. Hobday, R.J. Marshall, C.F. Murphie, J. Sotelo, T. Richards, D.R. Allan, T. Düren, F.X. Coudert, R.S. Forgan, C.A. Morrison, S.A. Moggach, T.D. Bennett, A computational and experimental approach linking disorder, high-pressure behavior, and mechanical properties in UiO frameworks, Angew. Chemie - Int. Ed. 55 (2016) 2401–2405, https://doi.org/10.1002/anie.201509352.

[195] H. Wu, T. Yildirim, W. Zhou, Exceptional mechanical stability of highly porous zirconium metal-organic framework UiO-66 and its important implications, J. Phys. Chem. Lett. 4 (2013) 925–930, https://doi.org/10.1021/jz4002345.

[196] Z. Hu, Y. Sun, K. Zeng, D. Zhao, Structural-failure resistance of metal-organic frameworks toward multiple-cycle CO2 sorption, Chem. Commun. 53 (2017) 8653–8656, https://doi.org/10.1039/c7cc04313a.